2016

Optically accessible bench-scale fast pyrolysis reactor for in-situ analysis using Fourier transform infrared spectroscopy

Eric Kok Hsien Chon
Iowa State University

Optically-accessible bench-scale fast pyrolysis reactor for in-situ analysis using Fourier transform infrared spectroscopy

by

Eric Kok Hsien Chon

A thesis submitted to the graduate faculty

in partial fulfillment of the requirements for the degree of

MASTER OF SCIENCE

Major: Mechanical Engineering

Program of Study Committee:
Terrence Meyer, Co-Major Professor

Xianglan Bai, Co-Major Professor

Young-Jin Lee

Iowa State University

Ames, Iowa

2016

Table of Contents

ACKNOWLEDGEMENTS iv

ABSTRACT v

CHAPTER 1. INTRODUCTION 1
1.1 Motivation 1
1.2 Objective and Contribution 2

CHAPTER 2. LITERATURE REVIEW 4
2.1 Composition of Biomass 4
2.1.1 Cellulose 5
2.1.2 Hemicellulose 6
2.1.3 Lignin 6
2.1.4 Organic Extractives 7
2.2 Biomass Pyrolysis 7
2.2.1 Introduction 7
2.2.2 Pyrolysis Classification 8
2.2.3 Reaction Pathway 10
2.2.4 Pyrolysis Reactors 11
2.2.5 Process Characteristics 14
2.2.6 Bio-Oil Characteristics 17
2.3 Fourier Transform Infrared Spectroscopy 19
2.3.1 Fundamentals of FTIR 19
2.3.2 Interferometer 19
2.3.3 Fourier Transformation of Interferogram to Spectrum 21
2.3.4 Infrared Spectral Analysis 23
2.3.5 Biomass Pyrolysis FTIR 25

CHAPTER 3. EXPERIMENTAL SETUP 27
3.1 Bench-Scale Pyrolysis Reactor 27
3.2 Sample Holder and Automated Insertion Device 30
3.3 Temperature Classification 32
3.4 FTIR Experimental Configuration 32

CHAPTER 4. RESULTS AND DISCUSSION 35
4.1 Temperature Profile Tests 35
4.2 Fourier Transform Infrared Spectroscopy Data 38
4.2.1 Red-Oak Spectra 38
4.2.2 Cellulose Spectrum Tests 41
4.2.3 Organosolv Lignin Spectra 43
4.3 Statistical Analysis of Spectra Shift 45
4.4 Fumed Silca Lignin 47
4.5 Evolution Tests 49
4.5.1 Sample Mass Analysis for O-H Stretch Functional Group 51
4.5.1 Sample Mass Analysis for C-H Stretch Functional Group 53
4.5.1 Sample Mass Analysis for CO_2 Functional Group 56
4.5.1 Sample Mass Analysis for C=O Stretch Functional Group 58

CHAPTER 5. CONCLUSIONS AND RECOMMENDATIONS 62
5.1 General Conclusions 62
5.2 Recommendations 63

REFERENCES 65

APPENDIX A. CELLULOSE SPECTRA PEAKS PLOTS 71

APPENDIX B. LIGNIN SAMPLES OF CO FUNCTIONAL GROUP PLOTS 72

APPENDIX C. EVOLUTION TEST PLOTS 73

ACKNOWLEDGEMENTS

A long project involves numerous people to complete from start to finish. I would like to take this opportunity to thank my major professor, Dr. Meyer for giving me this delightful opportunity and supervision for the duration of the project. I would also like to express my gratitude to Dr. Bai and Dr. Lee for being my co-major professor and committee member. I am blessed to have the privilege to work with my lab mates, Jordan Tiarks, Chloe Dedic, Dr. Micheal, and Patrick Sanderson. Their help with experimental setups and advice have been very supportive towards my project. I would also like to thank Dr. Chou of the Applied Sciences Department for being patient while working in his lab. I am grateful to my previous lab partner Nandith Chandy for lending me a hand, even though he is no longer involved in this project. He was very helpful in terms of providing valuable information and guidance on the research, and it was wonderful having the opportunity to work with him in the past. Many thanks to Deborah Schroeder, Neely Bushore, and Kristin Clemens for their administrative support. Finally, I would like to thank my parents for the support throughout my educational career. None of this would be possible without their support, and their support has been a great impact towards my work.

ABSTRACT

An optically accessible pyrolysis reactor was developed to analyze the *in-situ* reaction of biomass feedstock during the initial stage of fast pyrolysis. A Fourier Transform Infrared (FTIR) Spectroscopy, analytical instrument was modified to allow the light source to pass through the optical pyrolysis reactor for time-resolved measurements during the pyrolysis reaction. Cellulose, red oak, corn stove organosolv lignin, and a mixture of solid heat carrier with organosolv lignin were tested with the reactor. Evolution trends of the gas products and functional groups within the products were investigated as a function of time with the FTIR instrument. Residence times were regulated using a mass flow controller to allow different flow rates of sweep gas entering the reactor. Details of the reactor, including automated sample injection, temperature profile, and feedstock measurements are documented and discussed. The data collected in the experiments are shown to be useful for temporal analysis of pyrolysis products as a function of the type of feedstock. The analytical technique is proven to be repeatable and capable of capturing temporally resolved information that is otherwise difficult to obtain in conventional pyrolysis reactors. This can potentially provide improvement in understanding the kinetics of biomass fast pyrolysis.

CHAPTER 1. INTRODUCTION

1.1 Motivation

The demand and consumption of energy have grown in proportion to the global population. Currently, fossil fuels serve as the primary source of this energy for most practical purposes. However, fossil fuel energy sources are non-renewable and at the current rate of extraction will likely be depleted in a relatively short time. According to the Department of Energy and Climate Change (DECC), oil prices are projected to increase to $190 per barrel by 2035 [1]. Apart from an economic viewpoint, millions of tons of fossil fuels are burned every year, thus increasing environmental pollutants (e.g., CO_2, SO_x, and NO_x). This has led to major challenges due to global climate change. An approach that will help to alleviate these challenges is the development of biofuels, such as ethanol, from various biomass feedstocks and through various conversion processes.

Biomass refers to the organic material that has stored energy through the process of photosynthesis. Pyrolysis is a thermochemical conversion technology utilized to produce bio-oils from biomass and can be separated into three categories--slow, fast, and flash pyrolysis. Fast pyrolysis, in particular, is a thermochemical technology that yields the production of bio-oils through rapid heating in the absence of oxygen. It has been found that yields of 70-75 wt% of bio-oils can be produced via fast pyrolysis operating from the temperature range of 450°C to 500°C [3]. One of the first fast pyrolysis reactors was developed by Scott et al. in 1979 at the University of Waterloo to study how to obtain maximum yields of bio-oil production from aspen-popular wood [4]. Numerous aspects of fast pyrolysis such as temperature, heating rates, and vapor

residence times were characterized based on the yield of bio-oils. In prior work, researchers focused on maximizing yields of bio-oil from biomass feedstock through fast pyrolysis process without the benefit of *in-situ* spectroscopic measurements. Also, many studies based on pyrolysis have been conducted using Thermogravimetric analysis (TGA) to analyze the products of biomass thermal decomposition, but this analytic approach is orders of magnitude slower than the heating rates of practical fast pyrolysis systems.

The fundamental reaction mechanism of biomass during fast pyrolysis is poorly understood. Since fast pyrolysis occurs with seconds, it is difficult to investigate the reactions in time-resolved manner due to the limitations in instrumental and analytic techniques. This dissertation focuses on the development of an optically accessible, bench-scale pyrolysis reactor to allow *in-situ* temporally resolved studies of fast pyrolysis product evolution. In this work, the reactor is designed to allow Fourier Transform Infrared (FTIR) spectroscopy at data acquisition rates that can track the reaction through various stages of heating. By pairing the utilization of FTIR spectroscopy together with an optically accessible fast pyrolysis reactor, the goal of investigating fundamental reactions during fast pyrolysis of biomass feedstock is made possible.

1.2 Objective and Contribution

The purpose of this project is to develop an optically accessible, bench-scale fast pyrolysis reactor to allow direct investigation of the fast pyrolysis reaction process. Characterization of the reactor based on the requirements of fast pyrolysis includes the material used, heat transfer, temperature profile, heating rates, and residence times. The optically accessible pyrolysis reactor is then coupled with FTIR to study the temporally evolving characteristics of various types of biomass feedstock. Initial pyrolysis reactions of the biomass sample were analyzed with two different flow rates of heated nitrogen flowing through the pyrolysis reactor. A solid heat carrier (fumed silica)

is also mixed with biomass feedstock to prevent agglomeration and improve heat transfer; it is hypothezied that this will alter the agglomeration of lignin and potentially alter the product formation process. Such differences are tested in this work, and statistical analyses are used to evaluate system performance and sensitivity to potential systematic errors in spectral characteristics and time dynamics.

CHAPTER 2. LITERATURE REVIEW

2.1 Composition of Biomass

Biomass is a biological material derived from living organisms such as wood residue, agricultural residues and dedicated energy crops [5]. It is a well-known renewable source of energy production and is available worldwide. The fast growing cycle of biomass converts sunlight into food, a process called photosynthesis, and releases oxygen as a byproduct. Biomass has been widely used to generate fuel, chemicals, and energy with other thermochemical conversion techniques. Several biomass feedstocks have been used, but wood, in particular, is the oldest source people have used to generate heat through combustion. Through the history of energy consumption patterns in the United States, wood was the main energy source for most of the 1800's, followed by coal in the late 1800's and gas and oil in the latter part of the 1900's [6].

The common biomass used for the production of bio-oils through fast pyrolysis is lignocellulosic. It consists of three major compounds (cellulose, hemicellulose, and lignin) that are vital for the production. The cell wall of lignocellulose is divided into three separate zones: middle lamella, primary wall, and secondary wall [7]. The middle lamella is the layer formed during cell division and is shared by two adjoining cells. This section is composed primarily pectic substances and a small amount of protein [8]. Long oriented cellulose microfibrils together with a matrix of hemicellulose are formed in the primary wall [8]. The third zone of cell wall acts as a shield for plants. It is rigid and thick with the presence of lignin [8]. Figure 2.1 provides a clear image of the lignocellulosic cell wall. More detailed information will be provided in a later section. The ranges of weight % for lignin, cellulose and hemicellulose vary between 5-20, 30-50, and 10-40,

depending on the type of biomass [9]. Understanding the thermal decomposition of biomass requires understanding of how these components behave under practical pyrolysis conditions.

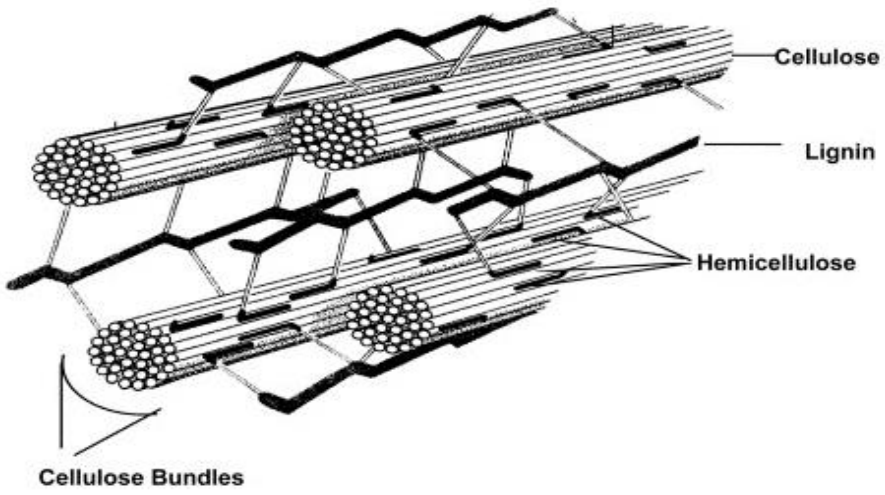

Figure 2.1.1: Macromolecular scale structure of plant cell wall [10].

2.1.1 Cellulose

Cellulose is a major component of lignocellulosic biomass and accounts for approximately 40-50 wt%. The glucose produced from plants is used to create cellulose. Cellulose is a linear polysaccharide polymer which consists of a long chain of glucose monosaccharide [11]. Groups of cellulose molecules are bonded by hydrogen bonds to form long chain bundles called micro fibrils, These chain bundles form the core of the complex that provides high tensile strength to the structure of a plant. The intermolecular and intramolecular hydrogen bonding of cellulose form a crystalline structure that is insoluble in most solvents, yet it becomes soluble at high temperature as sufficient energy is provided to break the hydrogen bond [12, 13]. With pyrolysis of cellulose at a temperature above 300°C, unstable material depolymerizes to primary volatiles, and levoglucosan is formed [12].

2.1.2 Hemicellulose

Hemicellulose constitutes approximately 25-35 wt% of lignocellulosic biomass. It is known as polyose and is considered a heteropolysaccharide that consists of numerous monomeric compounds (glucose, mannose, galactose, xylose, arabinose, 4-O-methyl glucuronic acid and galaturonic acid residue) [14]. Hemicellulose is amorphous and has a lower degree of polymerization. Thermal decomposition of hemicellulose occurs in the temperature range of 200-260°C. Pyrolysis of hemicellulose provides limited information due to its complexity, undefined structure, and inadequate isolation techniques [15]. Xylan has often been used as a substitute for hemicellulose due to the difficulty of extracting it from biomass. Hardwood contains a large amount of xylan whereas softwoods generally have more galacto-glucomannan [15].

2.1.3 Lignin

Lignin serves as a third major component behind cellulose and hemicellulose. It accounts for 16-25 wt% of the biomass, depending on either softwood or hardwood. The structure of lignin is an amorphous cross-linked resin that binds together the agglomeration of fibrous cellulosic components [12]. Lignin plays an important role in plant development and forms a shield to protect the cell wall against microbiological attack. A large mass of guaiacyl lignin can be obtained in softwood from the polymerization of coniferyl units, whereas guaiacyl-syringyl is naturally found in hardwood and is a copolymer of both coniferyl and sinapyl phenylpropane units [12]. Lignin is classified depending on the way it is isolated or extracted, therefore providing different physical and chemical properties. Pyrolysis of lignin can present an important challenge in the future of biofuels conversion. Lignin is the least reactive component in biomass and thermally decomposes in a temperature range of 280-500°C [16].

2.1.4 Organic Extractives

A small amount of the organic material can be extracted from lignocellulosic biomass. Their function is of transitional metabolism that defends against microbiological assault. Such examples of extractives include fats, waxes, alkaloids, proteins, phenolics, simple sugars, pectins, mucilages, gums, resins, terpenes, starches, glycosides, saponins, and essential oils [12]. These organics can simply be obtained by the extraction using either polar or non-polar solvents.

2.2 Biomass Pyrolysis

2.2.1 Introduction

Biomass technologies have attracted considerable interest over the years. Several types of technologies use biomass for generating electricity, co-firing in boilers, and making fuels for transportation purposes. The main five bio power systems are co-firing, direct biomass combustion, biomass anaerobic digestion, biomass gasification, and biomass pyrolysis [17]. Biomass pyrolysis is a process where biomass are heated rapidly at a temperature of 450°C to 550°C in the absence of oxygen. The heating rate is the key to differentiating slow, fast, and flash pyrolysis. Charcoal is the main product of slow pyrolysis (low heating rates and long residence times), whereas condensable vapors and aerosols are formed in fast and flash pyrolysis, which can be converted into bio-oils through rapid cooling and condensation. Biomass fast pyrolysis utilizes high heating rates of 100-1000°C/s at short residence times (1-3 s). The main goal of fast pyrolysis is to maximize the the production of condensable vapors to form bio-oils. Bio-oils obtained from biomass pyrolysis can be used with or without prior upgrading. They have been developed as an alternative source of fuel that helps to reduce the dependency of fossil fuels. Fossil fuels are formed as a result of natural actions (heat and pressure) on the fossilized matter for a million years; therefore, they are limited and cannot be recycled for near-term use. Bio-oils also utilize carbon

dioxide for growth so that the carbon dioxide that is emitted during combustion is naturally recycled [16]. Energy sources like fossil fuels increase carbon dioxide when burned, further increasing the greenhouse effect. Many studies have been conducted on the development of pyrolysis reactors to optimize heat transfer and produce the most liquid product in an efficient way. A later section will cover reaction pathway, pyrolysis classification, process characteristics, and bio-oil characterization.

2.2.2 Pyrolysis Classification

Slow Pyrolysis: Slow pyrolysis is categorized by low heating rates coupled with long residence times, thus favoring the formation of char products. This system operates at temperatures ranging from 300-500°C, with heating rates of 0.1 to 2°C/s [23, 24]. Due to longer residence times, primary products experience secondary reactions. Recombination or re-polymerization reaction will take place once the primary reactions have occurred [24]. At the end of slow pyrolysis, tar and char are collected from the reactor for further use of study.

Fast Pyrolysis: Due to high heating rates and slow residence times in fast pyrolysis, large amounts of vapors and aerosols, as well as smaller amounts of charcoal and gases, are produced from finely ground biomass feedstock. The usual target heating rates of biomass are 100-150°C/s inside a chamber operating at a temperature of 550°C. Residence times play an important role in yielding bio-oils, with a total of 75-80 wt% of bio-oils yielded via fast pyrolysis at short residence times (~1s) [25, 26]. However, to produce bio-oils in large scale reactos to be used as commercial fuels, longer residence times (~5s) are typically required [25]. Liquids production from fast pyrolysis is currently of research interest as the liquids have the potential of being upgraded to other fuels for heating and power or upgraded to chemicals to be used for industrial purposes. Feedstock with lower content of ash yields more liquids [25]. A dark brown liquid is formed after rapid cooling

and has a lower heating value compared to conventional fuels [26]. High-quality vapors yielded from fast pyrolysis, such as ethylene, are commonly used to create alcohols or fuel (ethanol) through rapid cooling [12, 16].

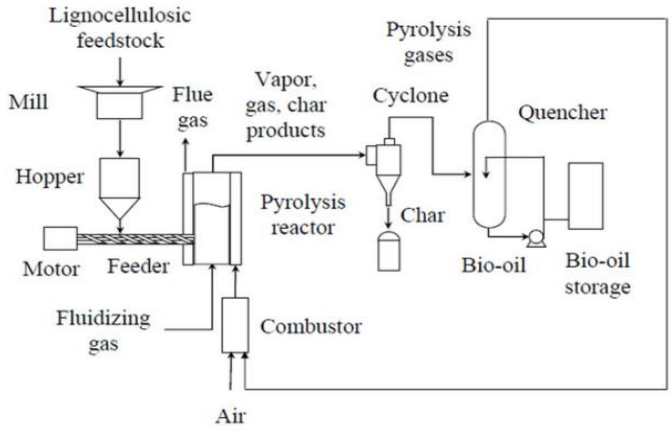

Figure 2.2.1: Schematic diagram of a fast pyrolysis system.

Flash Pyrolysis: Flash pyrolysis is a process that produces low contents of char and bio-oil, but high content of vapors from biomass. It has the potential to achieve a yield of ~70% vapors. This process operates at a temperature of higher than 550°C, as well as extremely high heating rates (>1000°C/s) and low residence times (<0.5 s) [27]. One major drawback of bio-oil via flash pyrolysis is the presence of pyrolytic water [24]. Yet, the presence of pyrolytic water in bio-oils have both positive and negative effects. A more uniform temperature profile exists, which is advantageous for combustion, thus leading to lower NOx emissions [28]. Conversely, the heating value and flame temperature of bio-oil is reduced, leading to an increase in ignition delay and a decrease in the combustion rate in some cases [28]. Steps to reduce the water content in bio-oil are required in order to make biomass flash pyrolysis competitive.

2.2.3 Reaction Pathway

Formation of bio-oils from biomass has attracted wide interest from all over the world. Biomass products are renewable and abundant, coming from living sources that can be replenished. During the heating of biomass, the color and weight of biomass are visibly affected. The color of biomass turns from white to brown then black, whereas mechanical strength and flexibility of biomass particles are weakened due to the weight lost [18]. Primary and secondary reactions occur on biomass pyrolysis products before, during, and after collection of bio-oils from the condensable vapors and aerosols produced.

Primary reactions of pyrolysis consist of dehydration or fragmentation [16]. Dehydration is prominent in slow pyrolysis that operates at a temperature below 300°C. Shafizadeh identified that reduction in molecular weight, subtraction of water, development of CO and CO2, and production of char occurs at low temperature [19]. On the other hand, depolymerization of biomass to anhydro-glucose compounds occurs in fragmentation operating at a temperature above 300°C [16, 19]. Condensable vapors are formed in this reaction, which are later converted to bio-oil through rapid cooling and condensation.

Volatiles produced in primary reactions can undergo secondary reactions with longer residence times and at lower heating rates, leading to cracking and recombination reactions. Cracking reactions result in lower molecular weight due to the breaking of chemical bonds of volatile compounds [20]. Lowering of molecular weight usually happens in fragmentation. Since cracking reactions occur within polymers or volatile compounds, it is difficult to differentiate which pathway reduces the molecular weight of compounds [21]. Conversely, recombination reactions increase the molecular weight by oligomerization of volatile compounds. Morf et al. suggested that the addition of a catalyst inside the reactor can prevent the formation of deposits on

the reactor surface [22]. These volatile compounds are the final products that yield bio-oils through rapid cooling, and it is important to avoid these secondary reactions.

2.2.4 Pyrolysis Reactors

A variety of pyrolysis reactors have been built throughout the years to pyrolyze various biomass feedstocks rapidly and effectively in order to optimize the yield of bio-oils. The factors that lead to an effective reactor depend on the amount of biomass feedstock that can be fed in as well as carrier gas. Furthermore, factors including heat transfer, temperature profile, and vapor residence time play an important role in the reactor performance. This section will discuss details about various pyrolysis reactors as well as their method of heating.

I. Ablative pyrolysis reactor: This is a reactor where it involves with large particles of biomass feedstock being pressed against a high relatively motion heated surface. The reaction depends on the heat transfer of conduction between the feedstock particles and the heated wall. A shearing action occurred in this process where oil film is generated from the thermal decomposition of biomass, and evaporates quickly to yield the production of bio-oils. A high pressure is achieved on large particles due to the centrifugal force and the operating temperatures of the reactor wall are less than 600°C [25, 26, 29, 30]. Inert gas is not required in this process, therefore, the processing equipment is small. However, there are some drawbacks with this pyrolysis reactor. This is a costly operation due to a surfaced area controlled system. In addition, this process is mechanically driven, resulting the reactor to be very complex [25, 26, 29, 30].

II. Fluid bed and circulating fluid bed pyrolysis reactor: This is a well-understood technology that yields large scale production of bio-oils through biomass pyrolysis. It is a reactor which utilizes a large bed of sand with hot gas transferring heat to biomass by a mixture

of conduction and convection [25, 26, 29, 30]. In order to obtain a good quality yields of bio-oils, a smaller size particles of less than 3 mm is used in this reactor due to heat transfer limitation within the particle [25, 29, 30]. Inert gas is required to transport vapor products and volatile in this process. Due to the high flow velocity of inert gas inside the reactor, the char formation can be removed easily. However, there is still a possibility that there is an increase of char content in the production of bio-oils. Techniques such as cyclone can be used for char separation.

Table 2.2.1: Reactor types and method of heating [25].

Reactor Type	Method of heating
Ablative Coil	Reactor wall heating
Ablative Mill	Reactor wall (disc) heating
Ablative Plate	Reactor wall heating
Ablative Vortex	Reactor wall heating
Circulating Fluid bed	In-bed Gasification of char to heat sand
Cyclone or Vortex	Reactor wall heating
Entrained Flow	Char combustion products
	Hot sand
Fluid bed	Heated recycle gas
	Hot inert gas
	Partial Gasification
	Fire Tube
Horizontal Bed	Fire tubes
Vacuum multiple hearth	Hearth heating
Rotating cone	Wall and sand heating
Stirred bed	Partial gasification of char
Transported bed	Recirculating hot sand heated by char combustion
Vacuum moving bed	Direct contact with hot surface

III. Entrained flow pyrolysis reactor: This is a relatively simple reactor design in which hot flows of inert gas transfer heat to biomass through convection. Experiments usually performed by freely dropping the sample cup into the reactor [32]. However, most reactor developments have not been successful due to the poor heat transfer from hot flow to biomass particle. Sufficient heat transfer can be achieved to biomass particle with high

flow of innert gas, but resulted in low liquid production [26,29,31]. The liquid production yielded in this reactor are usually low at 50-55 wt%[26].

IV. Fixed bed pyrolysis reactor: Due to the poor heat transfer and long vapor residence times, the main product in this pyrolysis reactor is charcoal. These reactors are separated into downdraft and updraft fixed bed reactors. The downdraft fixed bed reactor is characterized by slowly inserting biomass particles into a vertical shaft and contact with the same flow of the gas stream [26, 29, 32]. In contrast, updraft fixed bed reactor deals with biomass particles slowly inserted into the vertical shaft and contacted with counter flow of the gas stream [26, 29, 32]. Clean gas with low percentage of tar is produced in a downdraft fixed bed reactor, whereas updraft bed reactor produced dirty gas with high level of tars [26, 29, 32].

V. Rotating cone pyrolysis reactor: This reactor is mainly used as flash pyrolysis where a mixture of biomass and hot sand particles is placed at the base of the cone. Upon spinning of the cone, centrifugal force drives larger particles upward and to the lip of the cone where vapors are collected and further processed in a condenser [26, 32]. This process thermally decomposes biomass particles with rapid heating in a short residence time. Tiny amount of char is formed during pyrolysis and transferred into a char combustor, whereas sand particles are reused in the cycle [26, 32]. The requirement of carrier gas is relatively low in this pyrolysis reactor. Similarly, fine and dry biomass particles are required in order to yield 60-70% of liquid production [26, 32].

VI. Vacuum furnace pyrolysis reactor: The development of this reactor is not considered fast pyrolysis due to poor heat transfer rate of heat source to biomass. Biomass particles are thermally decomposed in short vapor residence times under low pressure in this reactor.

The vapor products from this pyrolysis process are then removed rapidly by the vacuum into a condenser where pyroltic oils are formed. This reactor includes the ability to feed in large biomass particles, however, a larger vacuum is required in the process which leads to higher expenses [25, 26]. Liquid production of 35-50% can be yielded from dry feedstock with high content of char formed [25, 26].

VII. Microwave pyrolysis reactor: In a microwave pyrolysis reactor, biomass particles are thermally decomposed within from the heat energy of a microwave heated bed. This reactor is connected directly to an electrical power source where eddy currents are generated to provide rapid heating to biomass particles [26, 33]. Continuous flow of inert gas is introduced into the reactor in order to maintain an inert environment.The effect of thermal gradients in biomass pyrolysis and secondary reactions can be analyzed as suggested by Bridgwater [26].

2.2.5 Process Characteristics

Many aspects still need to be taken into account, although pyrolysis has been established as a viable approach to the conversion of biomass to bio-oil. These features are essential to determine the performance, reliability, and consistency of biomass pyrolysis. The proportion of solid, liquid and gas products depends on the pyrolysis technique as well as reaction parameters. This section summarizes the importance of all these features.

- Temperature: The total product yield from woody biomass is affected by temperature inside a pyrolysis reactor. A large amount of char is produced with a lower temperature (<300°C), and between 500-550°C condensable and non-condensable vapors are formed from lignocellulosic biomass. This high temperature, on the other hand, causes a decrease in both residence time and char formation. A minimum temperature of 435°C must be

achieved for wood in order to yield at least 50% of quality liquid [25]. Bridgewater reported 55-60 wt% of bio-oils yield from a temperature around 480-520°C [26]. Yet, the underlying effects of temperature on the quality of the bio-liquid is poorly understood.

- Heat transfer: Heat transfer is divided into three main categories: conduction, convection, and radiation. Different types of pyrolysis reactors provide different kinds of heat transfer to pyrolyze biomass inside the chamber. In general, thermal conductivities of biomass are very poor, ranging from 0.03 to 0.4 W/mK [Kanury and Blackshear, 1970] [24]. Hence, heat transfer plays a major role in biomass thermal decomposition. Two forms of heat transfer are considered for heating biomass particles in fast pyrolysis to obtain vapors that can be converted into bio-oil. Gas-solid heat transfer is a process where heat is transferred from the hot gas to pyrolyze biomass through convection [25]. This process of heat transfer is commonly used in the entrained flow reactor. On the other hand, fluidized bed and ablative reactors have solid-solid heat transfer, which involves mostly conduction [25]. Only a small portion of radiation occurs for all pyrolysis reactors. Moreover, the particle size of biomass is also important. Smaller particles, usually in the micro scale, receive better heat transfer, thus providing a better yield of volatiles [36]. More detailed information on biomass particle size will be provided in the next section.

- Heating rate: Heating rate is a critical factor in biomass pyrolysis. It is a complicated process where it depends on time and also the location of biomass being pyrolyzed. In reality, as the reaction begins, maximum heating rates occur at the beginning of the process and slowly decrease with rising temperature inside the chamber [37]. Formation of char and vapors occurs at any temperature inside the pyrolysis reactor. However, heating rates together with temperature determine the wt% of products formed. Maximum yield of char

is formed at low heating rates (1-2°C/s) coupled with low temperature, whereas high heating rates (~1000°C/s) tend to favor the gas production. This is due to insufficient time for the volatiles to escape from the reaction zone [16]. Bridgwater et al. have shown that 53 wt% of bio-oil is obtained from tires at a temperature of 470-540°C in 0.88 s [35].

- Feed preparation: Since all biomass feedstocks have very poor thermal conductivity, there are particle size limitations on biomass due to the heat transfer rate. An assumption is made where smaller size particles (usually in micro scale) are able to be heated uniformly. Smaller size particles are capable of achieving higher heating rates and temperatures during pyrolysis, thus producing larger wt% of vapors. In contrast, a large amount of char is formed with an increase of size particle. This is because volatiles do not have adequate time to escape from the reaction zone before cracking occurs. Furthermore, drying of biomass feedstock is necessary. Bio-oil usually generates 15% of water in fast pyrolysis with raw biomass [25]. Water content in bio-oil cannot be removed by distillation, and this affects the corrosiveness, stability and other liquid properties [25].

- Vapor residence times: Heating rates inside a pyrolysis reactor are affected by temperatures and vapor residence times. If high temperatures are kept constant, residence times determine the amount of vapors formed in secondary reactions. Scott et al. stated that residence times affect the yield of bio-oil for a given biomass feedstock, where shorter residence time provides a greater yield in bio-oil and less char and vapors produced [25]. To optimize the production of bio-oil to be commercially used for transportation, high temperatures and heating rates as well as low residence times (~5s) and smaller particle sizes of biomass are required [25].

- Char separation: Char is a dark residue that is formed by the devolatilization of biomass at low-temperature pyrolysis [16]. Char acts as a vapor cracking catalyst that will affect the products in fast pyrolysis, thus rapid separation is essential [26]. The presence of fine char will increase the aging of the final products. Various techniques have been developed to tackle this issue, with the cyclone method being commonly used for char separation. Hot gas vapor filtration is another promising technique that filters large amounts of char from hot vapor and permanent gases [38].

- Liquids collection: Gas products of biomass fast pyrolysis include aerosols, condensable and non-condensable gases. Rapid cooling and condensation is then used to transform them into homogenous liquid (bio-oil) for various purposes. The rate of cooling is important for the formation of bio-oils. Slow cooling rate leads to deposition of lignin-derived components, which causes liquid fractionation and blockage of pipelines and heat exchangers [26]. Hence, quenching or interaction with cool liquid is often applied in bio-oil condensation to prevent this problem [26]. Bridgwater et al. stated that the transfer line of vapors from the reactor to the liquid collection system should be kept at temperatures >400°C to reduce liquid collection and deposition [25].

2.2.6 Bio-Oil Characteristics

Vapor products produced from fast pyrolysis turn into a liquid phase (bio-oils) via rapid quenching or contact with the cool liquid. Bio-oils are the potential substitute for fuels used in boilers, gas turbines and engines. Bio-oils are dark brown liquids comprised of a complex mixture of oxygenated hydrocarbons, typically with fine particles of char [26]. Bio-oils contain numerous chemical functional groups such as guaiacol, syringol, carbonyls, phenolics, and carbonxyls [19, 39]. The heating value of bio-oils are 17MJ/kg, which is 50% lower than conventional fuels [19,

26]. This is due to the higher oxygen content present in bio-oil. Physical properties of bio-oil from biomass are summarized in the table 2.3.2.

Table 2.2.2: Bio-oil characteristics [21].

Moisture Content	25%
pH	2.5
Specific Gravity	1.2
Elemental Analysis	
C	56.40%
H	6.20%
O	37.10%
N	0.20%
S	<0.01%
Ash	0.10%
Higher heating value, HHV	22.5 MJ/kg
Higher heating value, HHV as produced	17 MJ/kg
Viscosity	30-200cp

Important issues associated with bio-oils are acidity and phase separation. Bio-oils are very acidic with a pH value of 2.5. Major damage will be done to pipelines and storage vessels due to stress corrosion cracking; therefore, corrosion resistance pipelines and storage tanks are required. A significant amount of metal concentration will be found in bio-oil if parts of the pyrolysis reactor are fabricated with metal besides using stainless steel material.

The viscosity of bio-oils increase over time due to physical and chemical variations, therefore phase separation may occur. This is the result of breakdown of micro-emulsion and chemical reactions in bio-oil. Aging of bio-oils occurs rapidly with higher temperature, but can be reduced by storage in a cooler place [40]. The addition of water content (<30%) can reduce the viscosity of bio-oil [16]. However, there is a limitation on the addition of water before phase separation occurs.

2.3 Fourier Transform Infrared Spectroscopy

2.3.1 Fundamentals of FTIR

Fourier Transform Infrared (FTIR) spectroscopy is a commonly used analytical method to provide information on sample molecular structure. Infrared spectroscopy is a technique that probes the vibration of atom molecules. The spectrum is obtained from FTIR by passing infrared radiation through a sample and determining what fraction of radiation is absorbed from the sample. The display of the spectrum is usually absorbance versus wavenumber, with peaks that correspond to different molecular bonds. The samples in the form of liquids, solutions, pastes, powders, films, gases and surfaces can be analyzed with appropriate choice of sampling method [42]. The infrared spectrum is divided into three sections: far infrared (<400 cm^{-1}), mid-infrared (400-4000 cm^{-1}), and near-infrared (4000-13000 cm^{-1}) [41]. Many studies have been conducted only in the mid-infrared region where molecular vibration is very active. However, far and near infrared regions are also useful as they provide information on certain materials. Most of the modern FTIR instruments present the spectrum with wavenumber increasing from right to left. Mercury cadmium telluride (MCT) is often utilized to improve the sensitivity of the detector, but it has to be cooled with liquid nitrogen to obtain the desired spectrum.

2.3.2 Interferometer

The basic principle of the interferometer is incoming radiation is split into two, making one of the beams travel a longer distance before coming back to recombine with another beam. The final beam that passes through the sample and detector is the recombined beam of two individual reflected beams. The most common interferometer used in FTIR spectrometry is the Michelson interferometer.

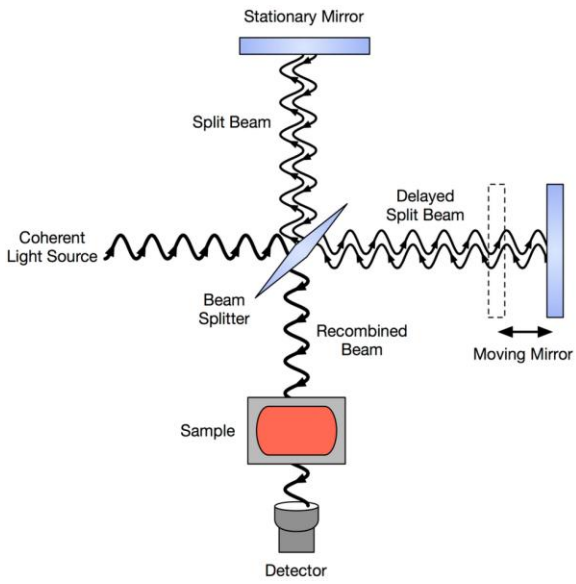

Figure 2.3.1: Michelson Interferometer [41].

As shown in the figure above, the Michelson interferometer utilizes beam splitter that directs the split beam into two perpendicular plane mirrors. One of the mirrors is in a stationary position, whereas the other is adjustable in a direction perpendicular to the plane to adjust the distance traveled before returning to the beam splitter. The moving mirror is a vital component in the interferometer and has to be properly aligned to create two path differences [42]. The beam splitter is a semi reflecting film that intersects the plane of these two mirrors. The material of beam splitter is usually potassium bromide or caesium iodide, coated with germanium or iron oxide for mid or near infrared region [41]. An ideal beam splitter would reflect 50% of the coherent light source to one of the mirrors and transmit another 50% to another mirror. Half of the beam reflected from the fixed mirror will transmit into the beam splitter where another half will be reflected back into the coherent light source. Two beams reflected from these mirrors will return to the beam splitter where interference occurs.

In reality, two possible outcomes of interference can occur from two returning beams. Constructive interference occurs when the phase difference between two waves (in radians) is an

even multiple of π, and destructive interference occurs when the phase difference is an odd multiple of π. For a difference in optical path length, δ, an integer, n, and a wavelength, λ, constructive interference occurs when

$$\delta = n\lambda \qquad (1)$$

Destructive interference occurs when:

$$\delta = \left(n + \frac{1}{2}\right)\lambda \qquad (2)$$

Equation (1) and (2) are obtained from references [41, 43].

2.3.3 Fourier Transformation of Interferogram to Spectrum

The interferogram with and without absorption by the sample can be transformed into spectra by using the Fourier transform. The Fourier transform is a mathematical method that is capable of decomposing a signal into frequency components characterized by sine and cosine waves. Equations that relate to spectral power density and intensity are given as:

$$I(\delta) = \int_0^\infty B(\bar{\upsilon}) \cos(2\pi\bar{\upsilon}\delta)\, d\bar{\upsilon} \qquad (3)$$

$$B(\bar{\upsilon}) = \int_{-\infty}^{\infty} I(\delta) \cos(2\pi\bar{\upsilon}\delta)\, d\delta \qquad (4)$$

$$B(\bar{\upsilon}) = 2\int_0^\infty I(\delta) \cos(2\pi\bar{\upsilon}\delta)\, d\delta \qquad (5)$$

Equation (3) and (4) were taken from references [41, 43], where $\bar{\upsilon}$ is the wavenumber.

Equation (3) and equation (4) are are recognized as a Fourier-transform pair. *I(δ)* shows the variation of power density as a function of path length difference, while B($\bar{\upsilon}$) express the variation of intensity as a function of wavenumber. Since *I(δ)* is an even function, equation (4) is rewritten into equation (5). Both can be converted into waves by Fourier transformation [41]. The

math description for Fourier transform can be complex and confusing. However, the Fast Fourier Transform (FFT) has been introduced in modern FTIR spectroscopy instruments to provide rapid calculations in the mid-infrared region.

The moving mirror in the interferometer is an important component that produces the interferogram. Interferogram obtained at the detector is an analog signal that has to be digitized before conversion into a spectrum by Fourier transformation. One possible error can occur when transforming digitized interferograms into spectra. The mathematical method of Fourier transform only assumes infinite boundaries, but transformation of the digitized the interferogram requires integration over a finite displacement [41]. This causes a series of positive and negative side lobes on the main band area. Apodization is used to address this error where side lobes can be removed by multiplying with a suitable function that causes the interferogram intensity to fall smoothly to zero [41, 42]. With this error corrected, Fourier Transform converts the interferograms into spectra.

Spectra from various interferograms are then added together. Two commonly used methods to increase signal-to-noise ratio (SNR) are smoothing and signal averaging [41-44]. The Golay-Savitzky smoothing function is a mathematical operation that draws a smooth curve through a set of noisy data [44]. Unfortunately, this function can lead to errors in the peak height due to the change in band shapes. Another well-known method for improving the spectrum is signal averaging [41, 44]. This process averages the spectra together, thus increasing SNR and improving the overall appearance of the spectrum. The amount of noise is proportional to the square root of the number of scans assuming random noise.

$$SNR \propto N^{\frac{1}{2}} \qquad (6)$$

However, if the noise is not random, the correlated signal will not be reduced and will appear as a definite signal in the spectrum.

The normal operating mode is to first record and store the spectrum without a sample (background), and then to record the spectrum with a sample in the beam path. This is to eliminate the background features and produce the spectrum due solely to the sample [42]. A typical FTIR background spectrum after purging can be seen in Figure 2.4.2, which shows a plot of intensity versus wavenumber (usually in units of cm^{-1}).

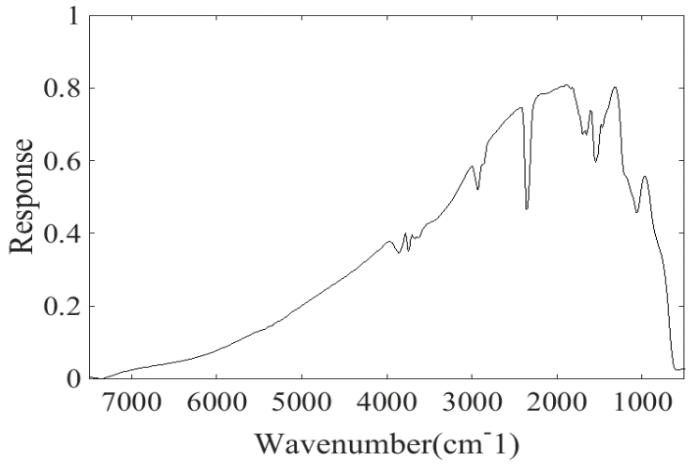

Figure 2.3.2: Background Spectrum after purging.

2.3.4 Infrared Spectral Analysis

Studies of molecular symmetry and group theory are vital when assigning infrared bands. The interaction of infrared radiation with matter is understood in terms of variations in molecular dipoles during vibration [41]. Vibrations of a molecule can be either stretching or bending vibration. Stretching vibrations can be further divided into two categories: symmetrical and asymmetrical stretching. Therefore, a particle that has a net dipole moment will be able to absorb the radiation energy. The larger the changes in molecular dipoles, the more intense will be the

absorption band. Stuart stated that symmetric vibrations of molecules are weaker compared to asymmetric vibrations due to an inability to generate strong dipoles [41].

Table 2.3.1: Functional groups of lignocellulosic biomass [45].

Wavenumber (cm^{-1})	**Functional Groups**	**Compounds**
3600-3000 (s)	OH stretching	Acid
2860-2970 (m)	C-H_n stretching	Alkyl, aliphatic, aromatic
2320	CO_2	Carbon dioxide
2150	CO	Carbon monoxide
1700-1730 (m)	C=O stretching	Ketone and carbonyl
1510-1560 (m)		
1632 (m)	C=C	Benzene stretching ring
1613 (w), 1450 (w)	C=C stretching	Aromatic Skeletal mode
1470-1430 (s)	O-CH_3	Methoxyl-O-CH_3
1440-1400 (s)	OH bending	Acid
1402 (m)	CH bending	
1232 (s)	C-O-C stretching	Aryl-alkyl ether linkage
1215 (s)	C-O stretching	Phenol
1170 (s), 1082 (s)	C-O-C strething vibration	Pyranose ring skeletal
1108 (m)	OH association	C-OH
1060 (w)	C-O stretching and C-O deformation	C-OH (ethanol)
700-900 (m)	C-H	Aromatic Hydrogen
700-400 (w)	C-C stretching	

Various techniques are used to interpret infrared spectra of a sample. Bands that appear in the infrared spectrum are usually assigned to specific bending or stretching of a bond, or deformation of a molecule, which is known as a group frequency [41-44]. The infrared region of the spectrum can be further divided into four classes and is generalized as: X-H stretching region (4000-2500cm^{-1}), triple bond region (2500-2000cm^{-1}), double bond region (2000-1500cm^{-1}) and

finally fingerprint region (1500-600cm^{-1}) [41]. The sharpness of the peak determines the infrared absorption response, and each peak wavelength in the spectrum represents a band that can be identified through spectral analysis. Yang et al. summarized a table of main functional groups for three major components of lignocellulosic biomass [45].

2.3.5 Biomass Pyrolysis FTIR

Numerous researchers have conducted studies on biomass pyrolysis. Some researchers have studied biomass pyrolysis based on the characteristics and simulations, whereas some of them focused on developing kinetic studies of biomass pyrolysis with various diagnostics and analytical instruments. An analytical instrument such as Thermogravimetric Analysis is often coupled with Fourier Transform Infrared Spectroscopy (TG-FTIR) and Gas Chromatography-Mass Spectrometry (GC-MS) to analyze gas products. Only a minority of researchers has conducted experiments with *in-situ* analysis of biomass pyrolysis using FTIR spectroscopy. FTIR spectroscopy is not typically applied with the *in-situ* evolution analysis. However, this method can be done with custom modification. Moreover, pyrolysis FTIR provides higher heating rates and functional group information that TG-FTIR cannot offer.

Yang et al. used TG-FTIR to analyze major components of lignocellulosic biomass and determined which gas species (H_2, CO_2, CO, CH_4, C_2H_6, and C_2H_4) were released at specific temperatures [45]. Fu et al. performed pyrolysis by dropping a sample basket inside a quartz tube reactor with a temperature of 900°C and a heating rate of 10^0C to investigate the evolution of pyrolysis products from agriculture residues [46]. Pyrolysis products of biomass samples were swept by nitrogen and analyzed using FTIR spectroscopy. Thermal decomposition studies performed by Leivens et al. tested heavy metal contaminated willow and branches [47]. Fumed silica is introduced into biomass feedstock in 1-1 volume ratio, and inserted into a horizontal quartz

tube reactor capable of achieving a heating rate of 35K/min. The reason behind adding fumed silica into biomass is to achieve uniform thermal decomposition of biomass. Vapor products are analyzed using both TG-FTIR and GC-MS instruments. Li et al. developed a method that rapidly heats cellulose and sweeps the gases into the FTIR cell with varying heating rates and residence times to study the product evolution [48]. Two heaters (movable and stationary) with temperature controllers were used in this reactor to study both primary and secondary reactions of cellulose. The movable heater is attached to a rail system to provide desired positions quickly.

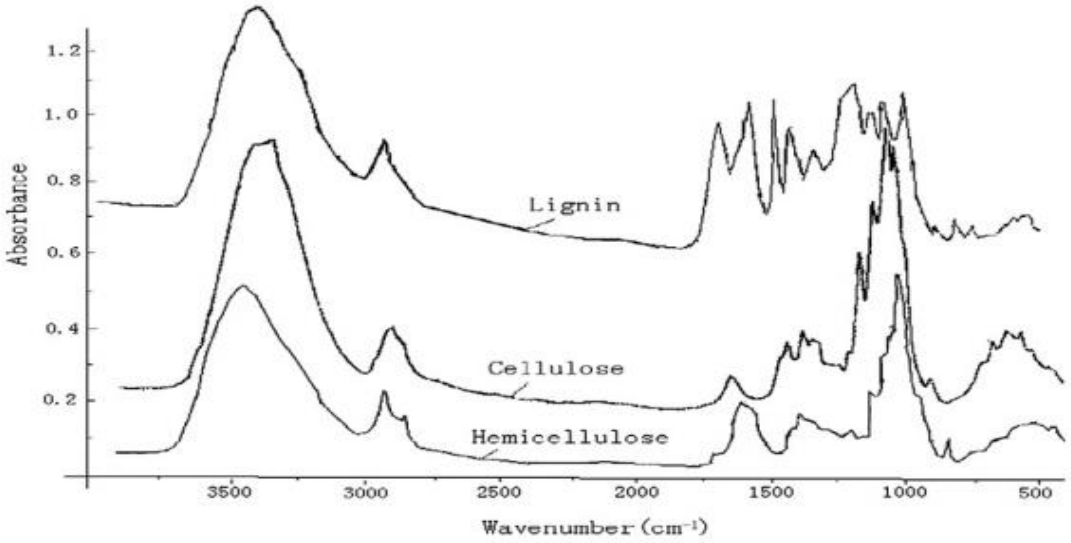

Figure 2.3.3: FTIR Spectrum of three components Lignocellulosic Biomass [45].

Yang et al. provided an FTIR spectrum of three major components of lignocellulosic biomass and is displayed in Figure 2.4.3. One can refer to Table 2.4.1 to study the functional groups according to wavenumber. To more closely replicate the pyrolysis conditions in practical reactors, it is of interest to more closely couple the reaction zone and measurement region, allow high heating rates through biomass injection into a heated cell, and minimize the spatial and temporal averaging of the measurement.

CHAPTER 3. EXPERIMENTAL SETUP

3.1 Bench-Scale Pyrolysis Reactor

As discussed in the previous chapter, pyrolysis reactors come in many shapes and sizes as well as sample feeding and heating methods. A variety of in-house pyrolysis reactors have been developed for various experimental needs. Small-scale pyrolyzers can be developed to analyze the fundamental of mechanism and product distribution from biomass pyrolysis. Often, small-scale pyrolyzers are attached directly with analytical instruments such as FTIR spectrometers, mass spectrometers, and gas chromotographs for product detection.

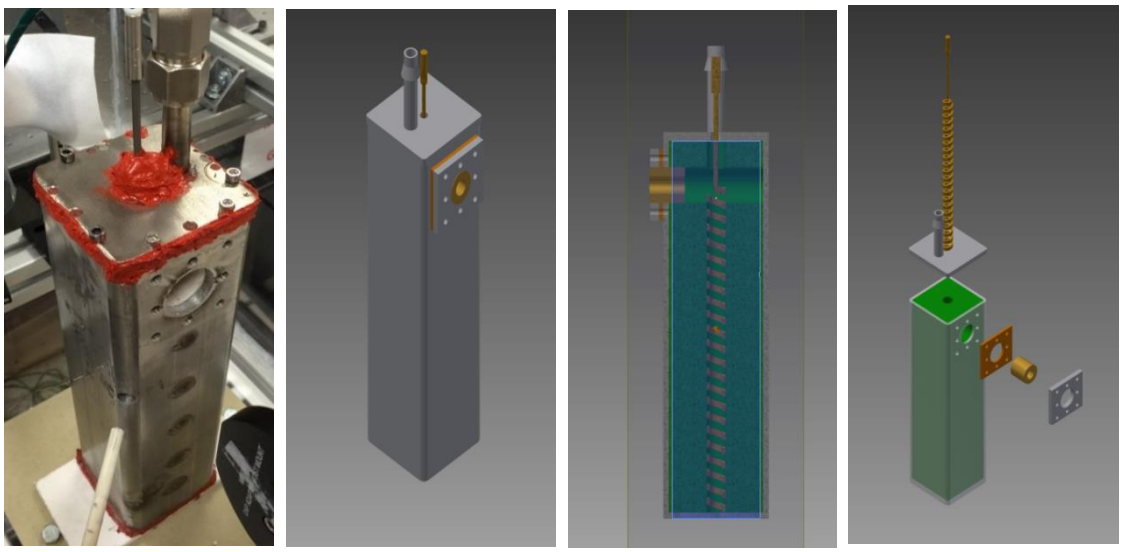

Figure 3.1.1: Pyrolysis reactor with optical access.

A bench-scale reactor was designed and fabricated for optical diagnostics to more closely replicate pyrolysis conditions. Figure 3.1.1 shows the model of the pyrolysis reactor. Design parameters of this reactor include the following: optical access for FTIR measurements with removable windows, ability to quickly reach and maintain a temperature of 550°C, a compartment

for biomass sample insertion, and variable flow rates entering the reactor to control vapor residence time.

The material used for the exterior of the reactor consisted of 304 stainless steel square tubing, with side dimensions of 76.2 mm and a height of 254 mm. Two 25 mm diameter holes were drilled in parallel onto the surface of the steel to provide compartments for IR transmission windows. Zinc Selenide (ZnSe) windows were chosen to place inside the compartment due to its ability to withstand the high-temperature environment. High-temperature silicon gasket sheets were placed in between the reactor windows and outer blocks for sealing purposes. Four macro glass-mica ceramic liners from McMaster-Carr were used to form a long hollow interior of the reactor to provide a nearly isothermal environment. Similarly, two 12.5 mm diameter holes were drilled through the ceramic and aligned with the center of 25 mm diameter hole for optical access. The dimension of the hollow cuboid was 20 mm x 20 mm with similar height to the exterior. A 9.5 mm diameter heater coil was slotted within the hollow cuboid and supported by a removable lid that covered the entire chamber. An exhaust vent was attached to the removable lid to allow vapor and volatiles to escape. Lastly, a 8.5 mm diameter hole was drilled near the bottom and through the corner of the reactor for sample insertion.

Two heating units were used for biomass thermal decomposition. The heater that supplied heat within the reactor is an Entherm 690 Watt, 965 mm straight resistance wire with a cross section of 2.2 mm x 4.2mm. This resistance wire heater was chosen due to its ability to bend into various shapes that allow space for IR transmission through the reactor. A desired coil shape was formed and fit into the hollow cuboid. The heater coil was powered by a Simran 110-220 V step-up transformer. Two K-type thermocouples from Omega were attached within the reactor to determine the temperature. The first and top thermocouple was located 38 mm away from the

center of the window. The bottom thermocouple, which was 75 mm below the center of the window, was connected to the temperature controller that varied the temperature by turning the heater coil on and off.

Another heating system consisted of a custom-built nitrogen heater located at the bottom of the reactor. The purpose of hot nitrogen gas was to assist in achieving desired heating rates to the biomass for thermal decomposition, along with sweeping vapor products to the exhaust vent. The nitrogen heater was made by wrapping heater tape (312 W) over a 1.8 m long, 9.5 mm diameter copper tube. Ceramic fiber sheet coupled with fiberglass fabric was used to coil around the nitrogen heater for better heat insulation. Likewise, the nitrogen heater was connected to the temperature controller, which achieved a temperature of ~550°C is achieved. Figure 3.1.2 displays both heating systems used in this experiment.

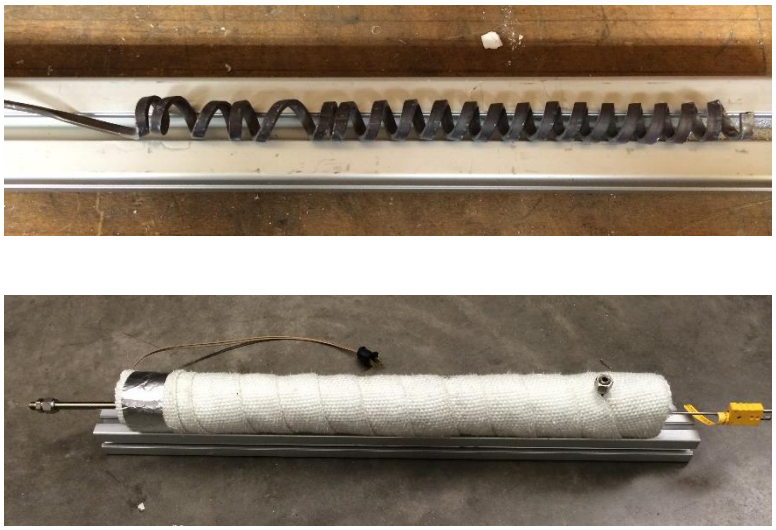

Figure 3.1.2: Heating units, including heating coil (top) and heated flow tube (bottom).

There was an issue where residue from pyrolyzed biomass fogging up both the inlet and outlet ZnSe windows rapidly. This fogging was caused by windows that did not reach the temperature of the interior of the pyrolysis reactor, thus resulting in condensation on the inner surface of both

windows. This issue was solved by adding another heater that flows desired heated nitrogen to both windows that has a similar temperature (~550°C) as the inside of the reactor.

The heating process began by switching both heating systems on and flow desired nitrogen into the reactor using a mass flow controller. This experiment was conducted inside an exterior acrylic box purged with cool nitrogen. The reactor was then allowed to reach steady state (~45 minutes). While waiting for the reactor to reach isothermal condition, the window heater was switched on and nitrogen was flowing through the heater to heat up the windows. Tests were carried out by inserting samples into the reactor, one at a time. Biomass samples were weighted using a laboratory balance and placed into a sample cup before insertion into the reactor. The next sub-chapter describes the device that holds the biomass samples.

3.2 Sample Holder and Automated Insertion Device

The design of the sample holder device is critical because it has to meet the following criteria: ability to withstand the reactor temperature, ability to hold and insert samples into the reactor, and ability to avoid pyrolysis from occurring before entering the chamber. Two different sizes of high-temperature alumina ceramic tube were chosen as sample holders for this experiment. The smaller ceramic tube (4.77 mm OD) had four bores. Two of the bores were used to hold steel wire of diameter 0.78 mm. Fine bare wire thermocouple was fitted into another two bores to monitor the temperature and heating rate of biomass thermal decomposition. This tube was then fitted into another ceramic tube with matching inner diameter. The larger ceramic tube was used to act as a plug when the sample holder was inserted into the reactor to prevent hot vapors from escaping the reactor. A steel foil of thickness 25 microns was cut and bent into a ‘V’ shape where both ends were sealed. The closed ends prevented samples from falling out of the foil during insertion into the reactor. The dimension of the sample cup was 1 cm x 0.5 cm. With this thickness

of the foil, high heating rates could be achieved for biomass samples. The size of sample cup is shown in the figure below.

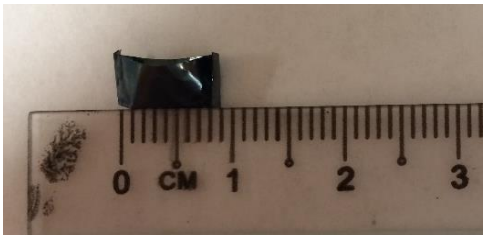

Figure 3.2.1: Sample cup size.

As shown in Figure 3.2.2 (left), the bent steel foil was then placed in between steel wires before attaching the assembly onto an automated insertion device powered by a solenoid in conjunction with a National Instruments cDAQ-9172. Variable speed of insertion could be achieved by applying a different voltage to the solenoid. This allowed for rapid insertion of samples into the heated environment and was repeatable for providing consistent results. Figure 3.2.2 (right) provides an image of the automated injection device.

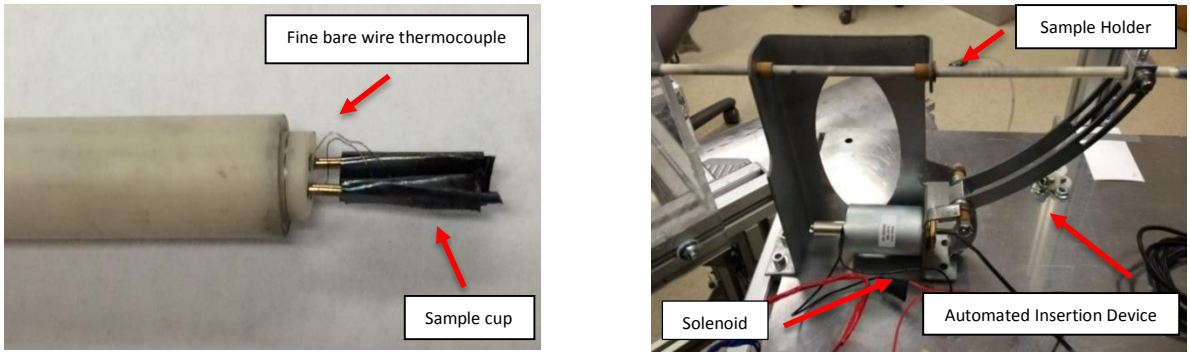

Figure 3.2.2: Sample holder (left) and automated injection device (right).

3.3 Temperature Classification

A digital thermometer from Omega was used to monitor the reactor temperature (top thermocouple) as well as the nitrogen heater. The tip of the thermocouples was placed at the center of the reactor to achieve centerline temperature at different measurement locations. It is noted that the temperatures of both heating systems were regulated using a temperature controller. Furthermore, the temperature of sample thermal decomposition at different flow rates was determined by a fine wire thermocouple attached in sample holder coupled with National Instruments cDAQ-9172. The temperature data were measured as a function of time and is reported in the next chapter.

3.4 FTIR Experimental Configuration

Given the size, height, and condition of the pyrolysis reactor, it cannot be placed internally on the sample compartment of the Varian 680 FTIR instrument. Therefore, a modification was made to the FTIR system in order to analyze the infrared absorption spectra of biomass samples.

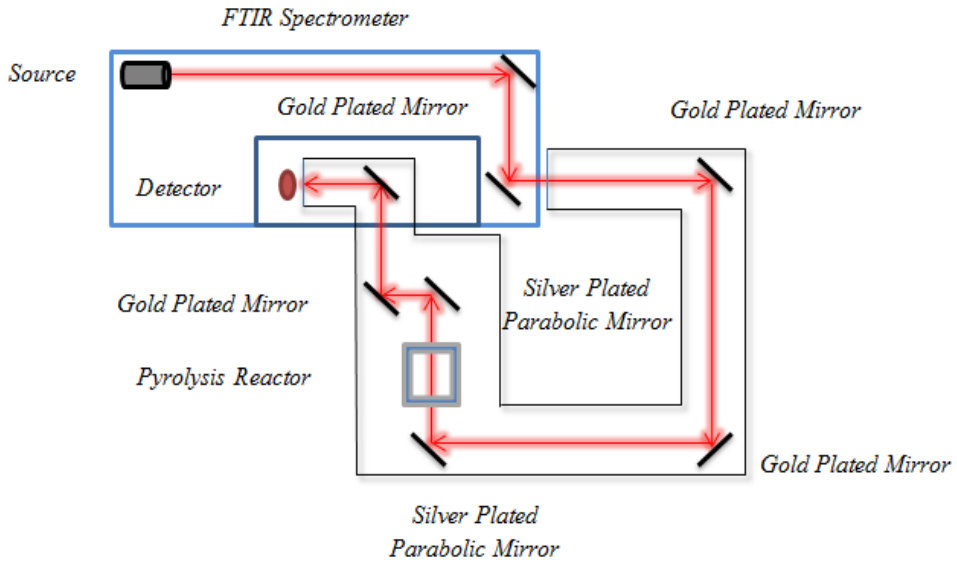

Figure 3.4.1: Modified Fourier Transformed Infrared Spectrometer.

A plane mirror was installed internally to draw the beam out of the Varian 680 FTIR system. According to Figure 3.4.1, six infrared reflective mirrors (4 gold and 2 silver mirrors) were installed to direct the beam from the source to the pyrolysis reactor and finally back to the detector. Two silver plated parabolic mirrors with focal lengths of 150 mm were placed at the entrance and exit of the reactor. The first parabolic mirror reflected the beam into the reactor, while the second parabolic mirror collimated the beam to the detector. Furthermore, two Zinc Selenide (ZeSn) windows were installed in the reactor to allow infrared transmission, and withstand temperatures. However, the transmission of IR for the ZnSe windows starts from wavenumbers of 4000 to 720cm^{-1}; thus, part of IR absorption cannot be analyzed in the mid-IR range. The entire system was enclosed with a 75 mm OD PVC pipe, to shield the beam path, and a sealed box of acrylic glass to encase the reactor. The encasement was purged with nitrogen gas to provide positive flow in order to prevent air and carbon dioxide from interrupting in the beam path when collecting background and sample spectra. A complete experimental setup is displayed in Figure 3.4.2, including the FTIR configuration, pyrolysis reactor, sample holder and injection, and purge encasement.

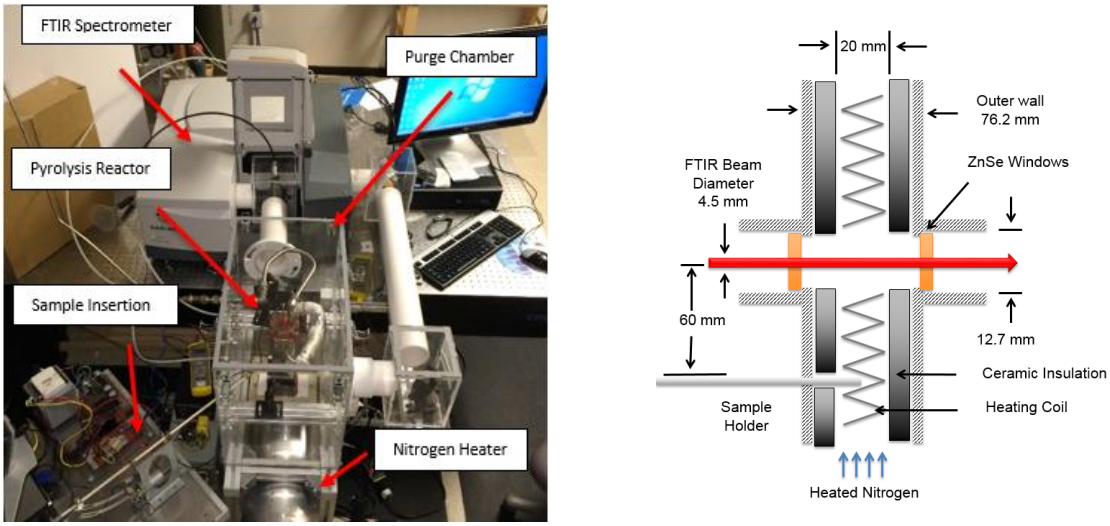

Figure 3.4.2: Overall FTIR setup showing purged beam path and chamber.

The original detector, Deuterium Tryglycine Sulfate (DTGS), was replaced with a Mercury Cadmium Telluride (MCT) detector within the FTIR spectrometer to provide high sensitivity in the mid-IR spectral range. This detector required liquid nitrogen cooling. Various residence times could be obtained with high sampling speed and spectral resolution. The data collection occurred with sampling speeds of 35.7 kHz (0.028 ms/scan) and 75 kHz (0.013 ms/scan). The two different speeds correspond to two different resolutions. A resolution of about 2 cm^{-1} is best achieved at lower sampling speed, while 8 cm^{-1} was achieved for higher sampling speed.

CHAPTER 4. RESULTS AND DISCUSSION

4.1 Temperature Profile Tests

Both the pyrolysis reactor and the nitrogen heater were preheated for 45 minutes with desired heated nitrogen gas flowing through the reactor. The total volume measured from the sample insertion point to the FTIR beam path through the pyrolysis reactor is approximately 25.2 mL. In this test, flow rates of 1 SLPM and 1.5 SLPM of heated nitrogen were chosen. These flow rates corresponded to maximum product residence times of 0.56 s and 0.37 s, as shown in Figure 4.1.1.

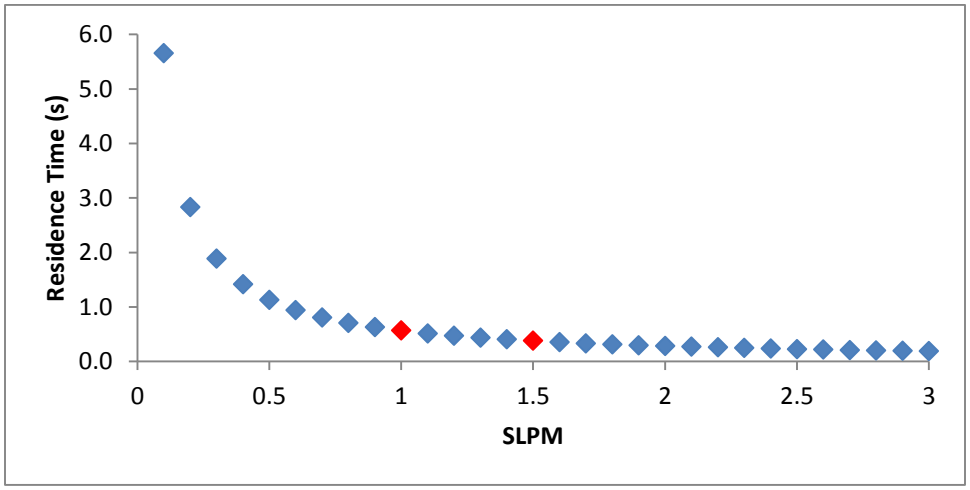

Figure 4.1.1: Product residence time versus flow rate in the reactor (SLPM).

Temperatures were obtained at 3 distinct locations, including the end point of the nitrogen heater and at a distance of 38 mm and 75 mm below the FTIR beam path. Both the bottom thermocouple (at 75 mm below the FTIR beam path) and nitrogen heater thermocouple were connected to a temperature controller where temperatures were regulated to 525°C. The third thermocouple was coupled to a National Instruments cDAQ-9172 to precisely measure the temperature inside the pyrolysis reactor. The data were then exported and plotted in Excel.

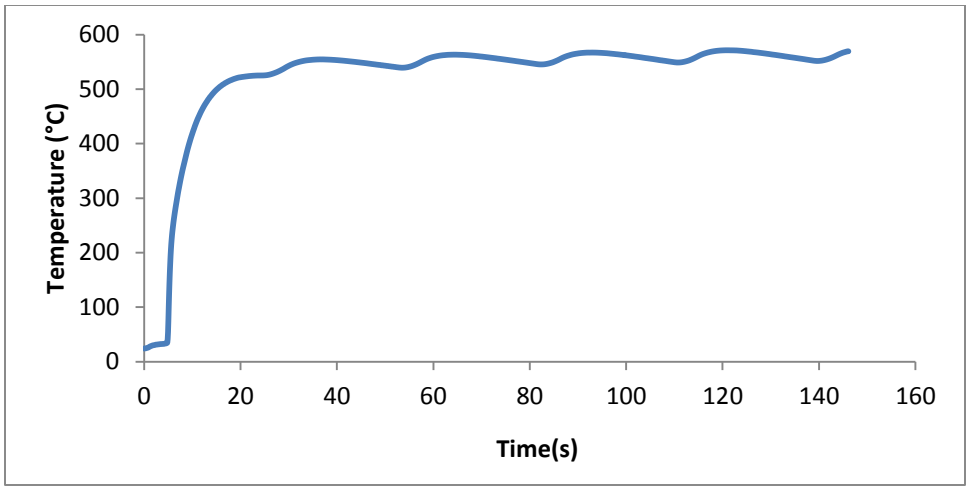

Figure 4.1.2: Temperature profile inside the pyrolysis reactor 38 mm below the FTIR beam.

The temperature profile is formed due to the temperature controller that varies the temperature by switching both heating systems on and off. The temperature obtained from the third thermocouple shows a higher temperature (~570°C), although both heating systems were regulated to 525°C. This is due to the buoyancy as hot air rises to the top of the pyrolysis reactor, thus resulting in an increase of temperature.

In order to test the heating rates of the sample cup at various flow rates of heated nitrogen, a fine wire thermocouple is used and attached in the sample holder. This can be seen in Figure 3.2.2 and 4.1.3. Stainless steel foil with a thickness of 25 microns is first bent into a "V" shape and attached in between the sample holder steel wires. The fine wire thermocouple is carefully placed where only the tip touches the surface of the stainless steel foil. Once the sample holder is complete, it is attached to the automated sample insertion device. Controlled by a National Instruments cDAQ-9172, the sample holder is inserted into the heated environment with a constant speed of 63.5 cm/second. Figure 4.1.4 provides a clear image of heating rates at different flow rates. It is important to note that the temperature of the sample holder may not represent the temperature of the sample itself, which may vary from the exterior of the sample to the interior.

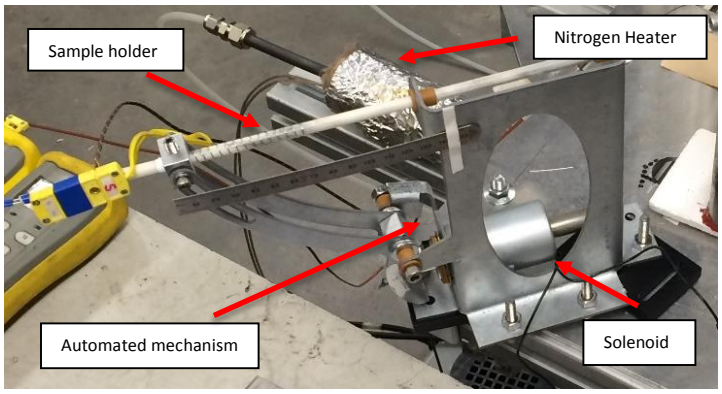

Figure 4.1.3: Automated mechanism used to measure the temperature of the biomass.

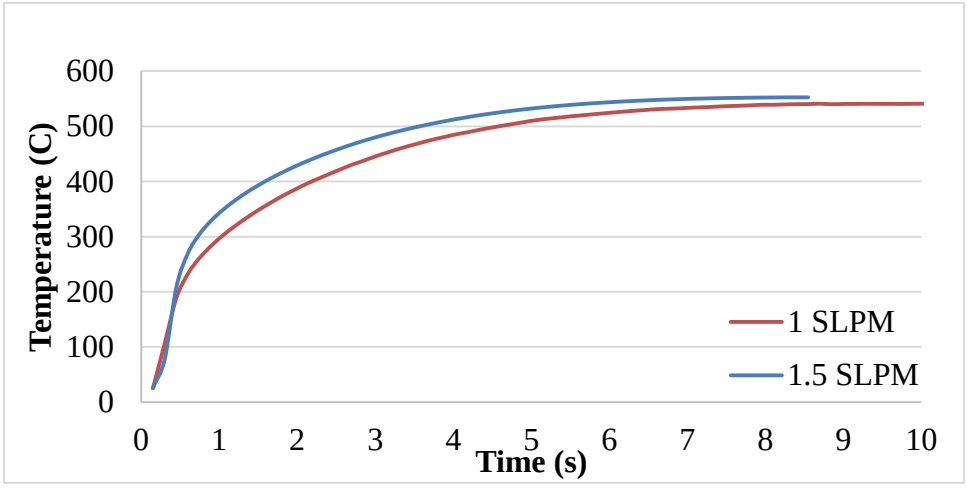

Figure 4.1.4: Heating rates of sample cup at various flow rates of heated nitrogen.

The heating rate for each flow rate was calculated from the time to reach 10% to 90% of their temperature. It is clearly shown that 1.5 SLPM of heated nitrogen flowing through the pyrolysis reactor provides a higher heating rate compared to 1 SLPM. The heating rate for 1.5 SLPM is <133°C/seconds while 1 SLPM produced <112°C/seconds. From the result of this test, the initial reaction of pyrolyzed biomass feedstock can be studied. The estimation of heating rate for the micropyrolyzer used by Dr. Robert Brown's students of Iowa State University is around 100°C/seconds for an operating temperature of 500°C inside the reactor.

4.2 Fourier Transform Infrared Spectroscopy Data

Four biomass feedstocks consisting of red oak, cellulose, organosolv lignin, and fumed silica lignin were tested in this experiment. The initial setup was to allow both heating systems to reach steady-state condition (~45 minutes) with heated nitrogen flowing from the bottom of the pyrolysis reactor. This experiment was conducted inside a purge box with a flow of cool nitrogen. Note that dry air, used initially, was replaced with nitrogen to purge the FTIR spectrometer due to issues with carbon dioxide contamination in the spectra. Biomass feedstocks were weighted precisely using a laboratory balance and placed into the sample cup before insertion of the cup in between the sample holder steel wire. Biomass samples were purged with nitrogen for a duration of 3 minutes before insertion into the reactor. The insertion of biomass sample into the pyrolysis reactor was regulated by a custom-built automated device powered by a solenoid. A voltage of 15 V is applied onto the solenoid to produce a constant speed of 63.5 cm/s. The Varian 680 FTIR software (Agilent Resolution Pro) initiates data collection once the sample holder is inserted into the heated zone. The biomass sample is left inside the pyrolysis reactor for 55 seconds before pulling it out.

4.2.1 Red-Oak Spectra

This experiment starts with 7 mg of red oak being injected into a reactor which is preheated to 550°C environment. In Figure 4.2.1, a spectral profile during the pyrolysis of 7 mg of red oak is plotted with respect to different measurement speeds (37.5 kHz or 75 kHz) and residence times (as dictated by 1 SLPM or 1.5 SLPM flow rates and fixed position above the sample). The spectra were obtained with a spectral resolution of 8 cm^{-1} at 75 kHz detection speeds and 2 cm^{-1} at 37.5 kHz. Background subtraction was applied to all spectra. These spectra show the product spectra 6 seconds after sample insertion from time series collected by the Agilent Resolution Pro software.

A 5 point boxcar digital comb filter was used to smooth all spectral plots. With ZnSe windows installed in the pyrolysis reactor, the detected Mid-IR range is from 4000-720 cm^{-1}.

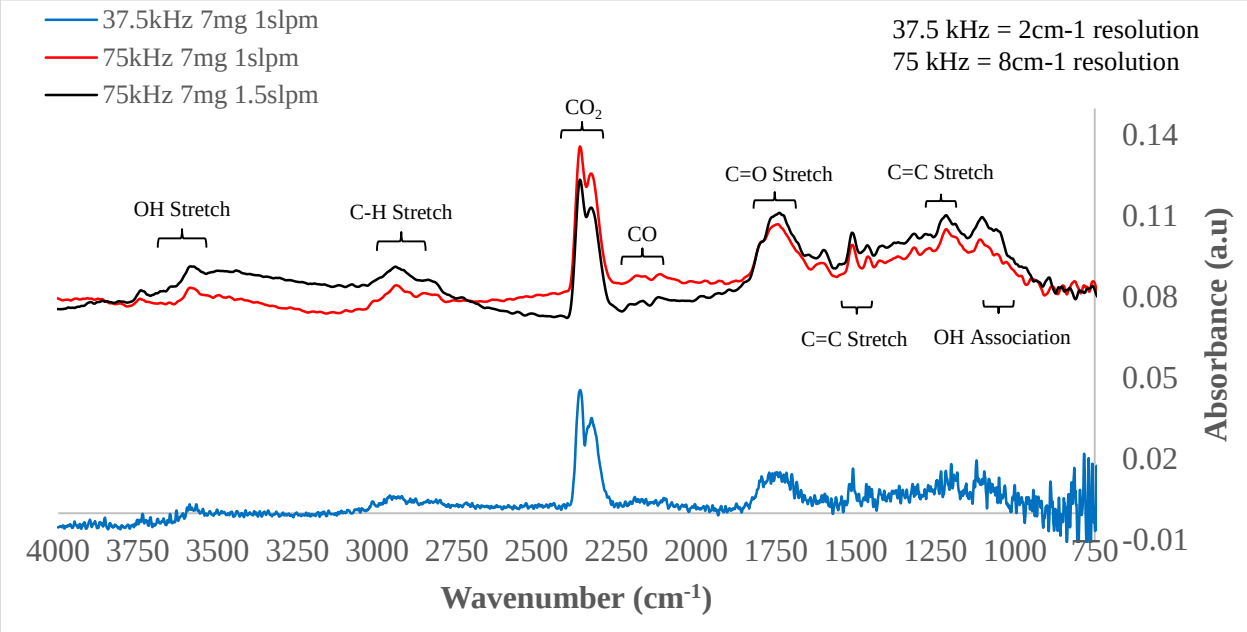

Figure 4.2.1: Red-oak spectra comparison at varying detection speed for a sample load of 7 mg. Residence time is higher for 1 slpm compared with 1.5 slpm of heated nitrogen.

The absorbance peaks in Figure 4.2.1 appear at 3590 cm^{-1}, 2920 cm^{-1}, 2360 cm^{-1}, 2325 cm^{-1} 2150 cm^{-1}, and 1750 cm^{-1}. The first absorbance peak at 3590 cm^{-1} is due to O-H stretching, while C-H stretching occurs at the second peak at 2920 cm^{-1}. The most prominent absorbance peak corresponds to the asymmetric stretch of CO_2 at 2360 cm^{-1} and 2325 cm^{-1}, while a small peak for CO appears at 2150 cm^{-1}. The last peak at 1750 cm^{-1} is attributed to the functional groups for C=O stretching. Additionally, three peaks arise in the fingerprint region (1500-750 cm^{-1}). Based on the literature, C=C stretching and O-CH_3 functional group are found in the first peak (1450 cm^{-1}) of the fingerprint region. The second peak located at 1205 cm^{-1} has a C-O stretching term which appears during pyrolysis. The final peak occurs near 1103 cm^{-1}, which corresponds to the OH association functional group.

Lower speed spectra (blue plot) was tested in this experiment due to its ability to provide better resolution (2 cm^{-1}) where spectra was obtained with every one wavenumber. However, the plot for lower speed spectra produced significantly more noise around the fingerprint region (1500-750 cm^{-1}) without any apparent improvement in the spectral characteristics. Therefore, evolution tests for all tests were analyzed at higher speed. The residence time, with 1 slpm being longer than 1.5 slpm, did not seem to have a significant effect.

The evolution of red-oak spectra in time during the reaction is plotted in Figure 4.2.2 in 1 s increments from 3-9 s starting from bottom to top. These spectra were taken at the higher detection speed of 75 kHz and longer residence time (0.56 s) with a flow of 1 slpm. This provides information about the dynamics of the product formation processing by showing the evolution of absorbance from different functional groups.

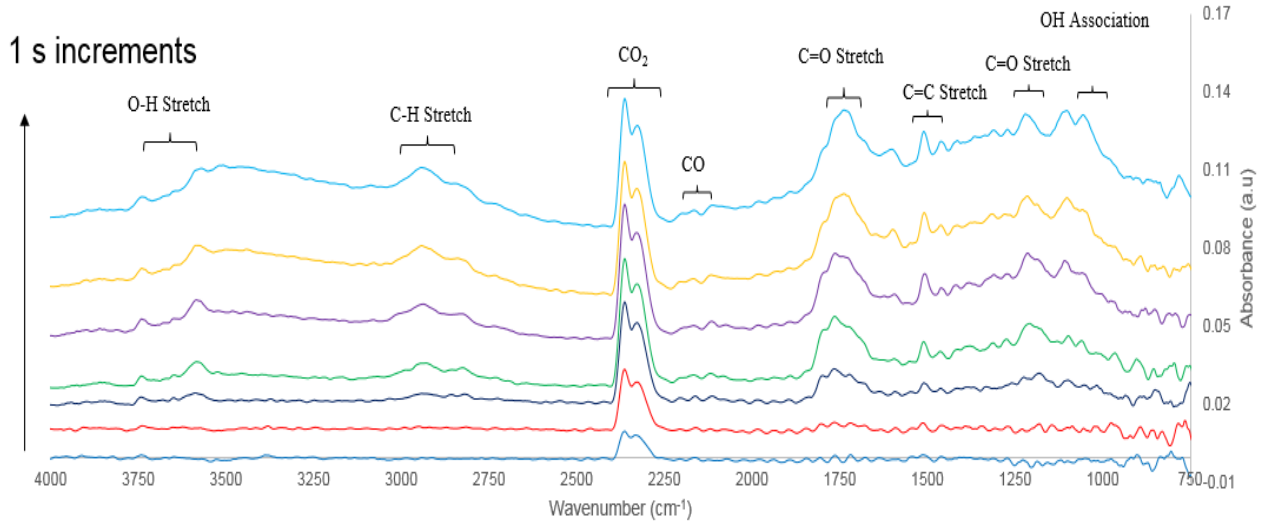

Figure 4.2.2: Red-oak spectra evolution in increments of 1 s from 3-9 s (bottom to top) after biomass insertion. Travel time from biomass sample to measurement location is 0.56 s.

The data in Figure 4.2.2 show that few of the functional groups other than CO_2 are detectable at 3 s after insertion of the biomass sample. This includes a travel time of 0.56 s from

the sample holder to the measurement volume, meaning that the products were produced at the sample location about 2.44 s after injection corresponding with a sample holder temperature of about 412°C according to Figure 4.1.4. Other functional groups begin to appear at about 4 s after insertion, with the products generated when the biomass sample holder should be at about 485°C.

4.2.2 Cellulose Spectrum Tests

Cellulose from Sigmacell was used in this experiment as a standard feed. The particle size of this sample was 50 µm. The procedure was carried out in a similar way as red oak. The IR spectra were taken at a time resolution of 0.106 seconds for higher speed and 0.381 seconds for lower speed. The time resolution is fixed with the given speed.

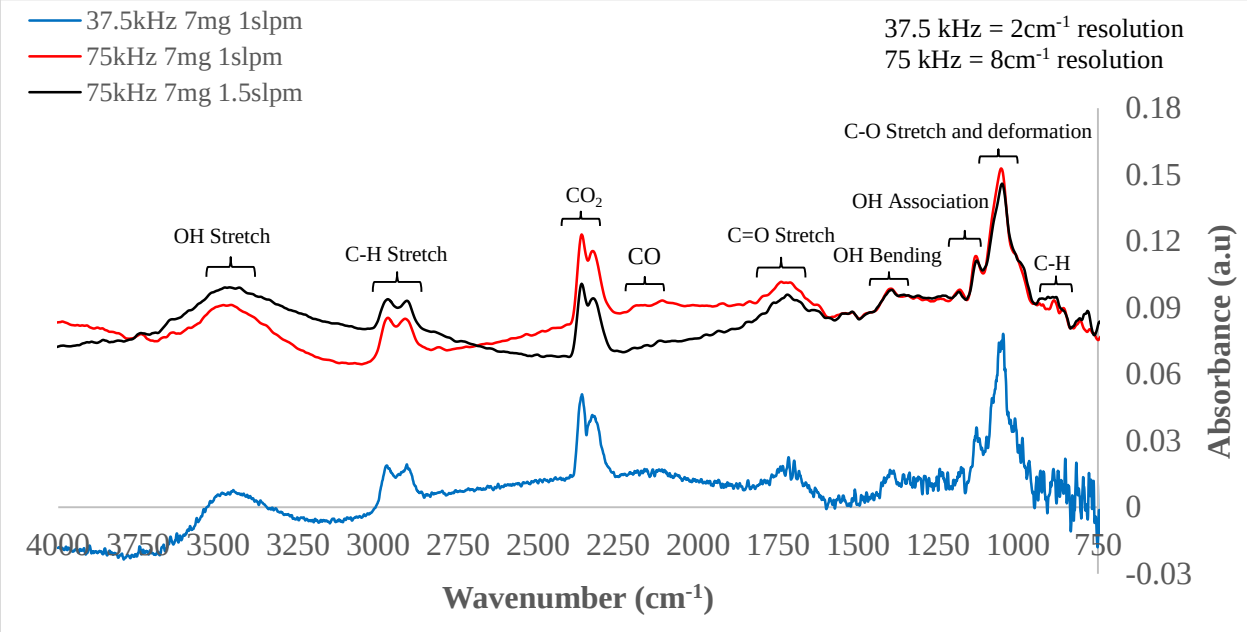

Figure 4.2.3: Cellulose spectra comparison at varying detection speed for a sample load of 7 mg. Residence time is higher for 1 slpm compared with 1.5 slpm of heated nitrogen.

As suggested from R. Bassilakis et al., the concentration of various gas products will reflect the change in IR peak height [45, 49]. Vapor products released from cellulose mainly occured at a

reactor temperature of 370^{0}C. Spectra of cellulose pyrolysis were extracted at 8 seconds and are displayed in Figure 4.2.3. Obvious absorption peaks are around 3460 cm^{-1} (OH stretch), 2970 and 2910 cm^{-1} (CH stretch), 2360 cm^{-1} and 2320 cm^{-1} (CO_2), 2130 cm^{-1} (CO), and 1720 cm^{-1} (C=O stretch). Cellulose produced the least amount of CO_2 compared to both red oak and organosolv lignin (where spectra will be provided later in the next subtopic). The contribution of CO from pyrolyzed cellulose was minor. A few interesting peaks were found around the fingerprint region of pyrolyzed cellulose: 1411 cm^{-1} (OH bending), 1050 cm^{-1} (OH association), and 875 cm-^{1} (C-H). The highest absorbance peak occurs at a wavenumber of 1050 cm^{-1} due to C-O stretching and deformation. The cellulose spectra produced the same feature when comparing with the FTIR spectrum from Yang et.al, except for the production of CO_2 [50]. The evolution of cellulose spectra in time during the reaction is plotted in Figure 4.2.4 in 1 s increments from 4-10 s starting from bottom to top.

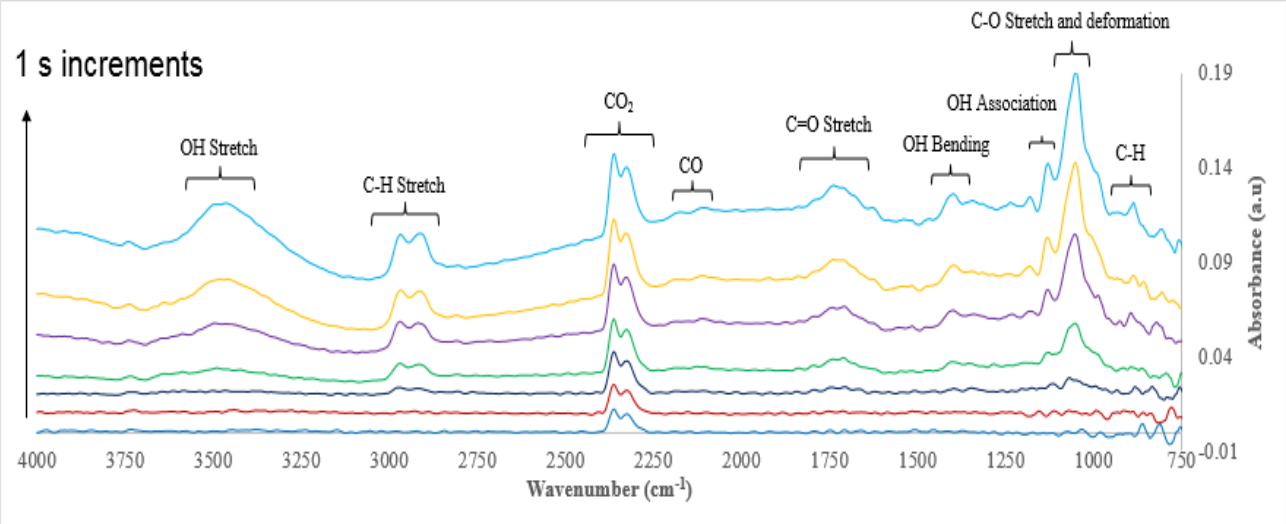

Figure 4.2.4: Cellulose spectra evolution in increments of 1 s from 4-10 s (bottom to top) after biomass insertion. Travel time from biomass sample to measurement location is 0.56 s.

These spectra were taken at the higher detection speed of 75 kHz and longer residence time (0.56 s) with a flow of 1 slpm heated nitrogen from the bottom of the reactor. Similar to red-oak spectra, the data in Figure 4.2.4 show that most of the functional groups are not detectable at 4 s after insertion of cellulose into the preheated reactor except for CO_2. Functional groups begin to appear at about 5 s after sample insertion where vapor products are generated with sample holder reaching temperature of 420°C according to Figure 4.1.4.

4.2.3 Organosolv Lignin Spectra

The third set of tests deals with organosolv lignin samples. Yang et al. pointed out that organosolv lignin was the most difficult to decompose and decomposition occurs at a very wide temperature range (160-900°C) [45]. Since organosolv lignin has a very poor thermal conductivity, smaller size particles (<60 µm) were used there to achieve higher heating rates.

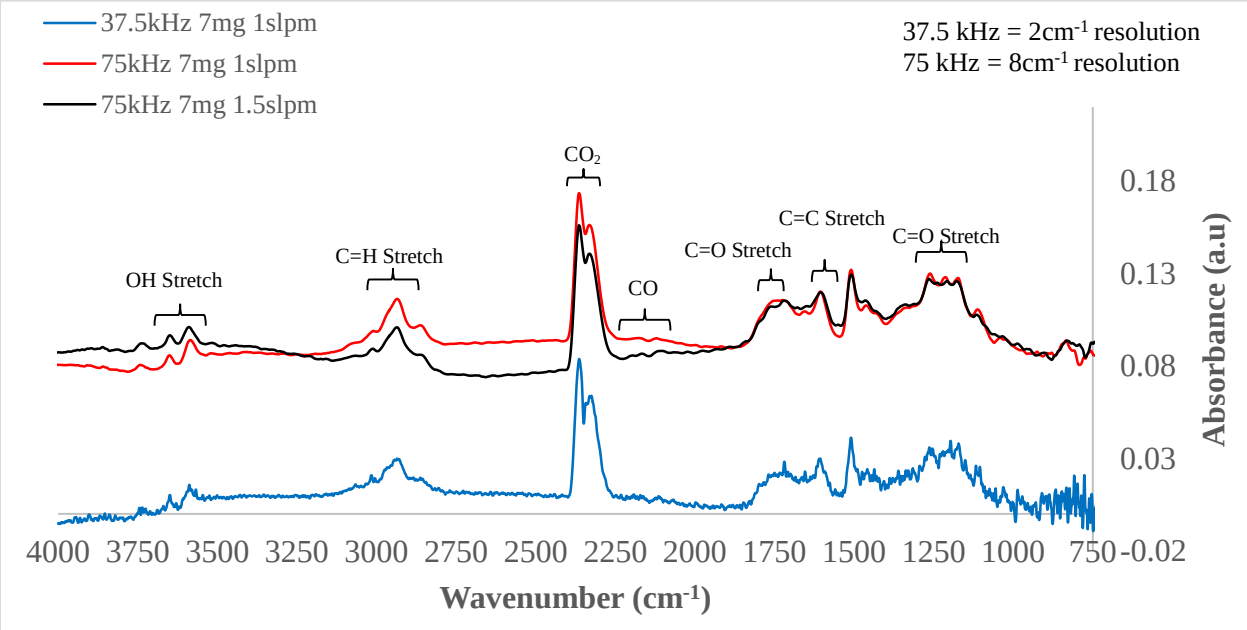

Figure 4.2.5: Organosolv lignin spectra comparison at varying detection speed for a sample load of 7mg. Residence time is higher for 1 slpm compared with 1.5 slpm of heated nitrogen.

As before, organosolv lignin samples were first weighted at 7 mg and transferred to the sample cup before electronically controlled insertion into the hot reactor. The data in Figure 4.2.5 show organosolv lignin spectra were extracted at 8 seconds for different speeds and residence times. A few peaks occurred from pyrolyzed organosolv lignin where it falls in the functional groups similar to red oak and cellulose at a wavenumber of 4000-1750 cm^{-1}. Carbon dioxide (2360 cm^{-1} and 2330 cm^{-1}) has the highest absorbance peak compared to cellulose. The C-H stretch is generated by hydrocarbons such as methane in the methoxy group (CH_3-O-), and its peak at 2920 cm^{-1} located to the left of CO_2 [45, 46]. The concentration of CO at 2130 cm^{-1} for organosolv lignin appears to be the lowest at a temperature 550°C, however, the concentration will increase with higher temperature (~700°C) [45]. Another two peaks arise at 1725 cm^{-1} and 1600 cm^{-1}. These two peaks correspond to C=O stretching and C=C stretching. Compounds of ketone, carbonyl and aromatic compounds can be found in both functional groups [45]. C-O stretch of the phenol compound is observed at the broad absorbance peak ranging from 1250-1165 cm^{-1}. With the complex structure of lignin, many functional groups such as phenol and guaiacol may be present in this range, as suggested from Liu et al. [51]. Spectra for fumed silica lignin produced exactly the same functional groups as organosolv lignin, and these are not presented here. However, there are some interesting differences in the time evolution between three different types of lignin that be will analyze in evolution sub-chapter.

The evolution of organosolv lignin spectra is plotted and shown in Figure 4.2.6, with different functional groups appearing in time. These spectra were taken from 2-8 s, with an increments of 1 s at a higher detection speed of 75 kHz and shorter residence time (0.38 s) with a flow of 1.5 slpm heated nitrogen. Most of the functional groups begin to evolve at 4 s after insertion, with the products generated where the sample cup reaches a temperature of 510°C.

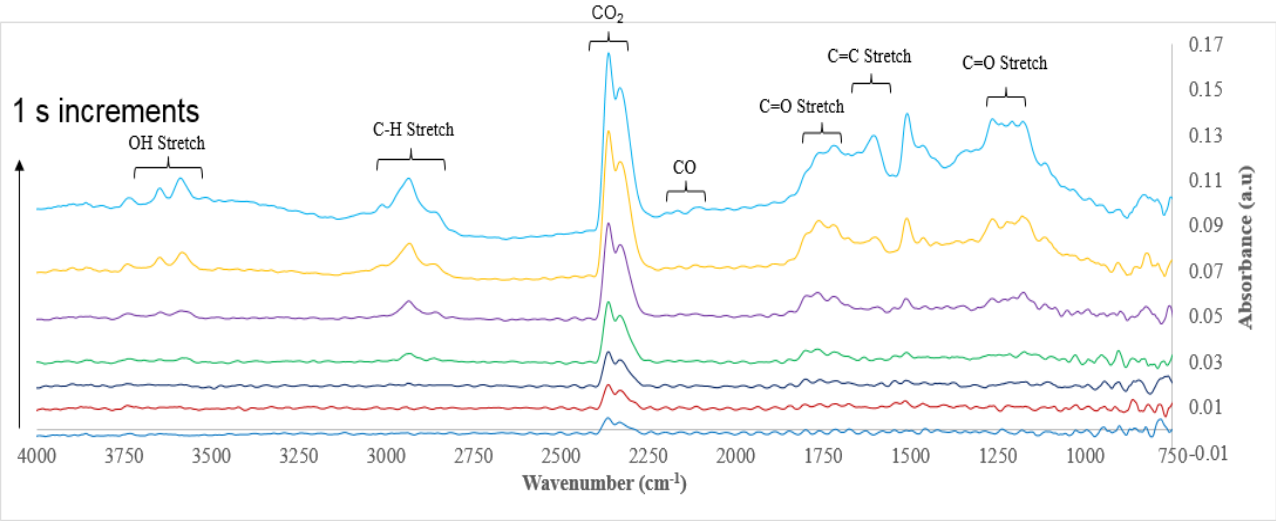

Figure 4.2.6: Organosolv lignin spectral evolution in increments of 1s from 2-8 s (bottom to top) after biomass insertion. Travel time from biomass sample to measurement location is 0.38 s.

4.3 Statistical Analysis of Spectra Shift

Spectra for various biomass samples acquired from the previous section were baseline-corrected using a segmented linear baseline. With an increment of 1 s in all spectral evolution graphs, peaks of different functional groups seem to be at the same location. The wavenumber intervals (x-axis) presented in all spectral evolution graphs are 250 cm^{-1} apart. However a possibility of spectra shift might occur as the temperature varies over time. One possible approach to the issue is by marking the highest point of the peaks from different functional groups with respect to time, and analyze them statistically. This provides insight as to whether spectra shift over time, and what suitable window range could be used to capture those peaks. Since temporal spectra of organosolv lignin were acquired, this test begins by selecting peaks of different functional groups evolved over time. The location of selected peaks was around 3467 cm^{-1} (OH stretch), 2933 cm^{-1} (C-H stretch), 2330 cm^{-1} (CO_2), 2157 cm^{-1} (CO), and 1765 cm^{-1} (C=O stretch).

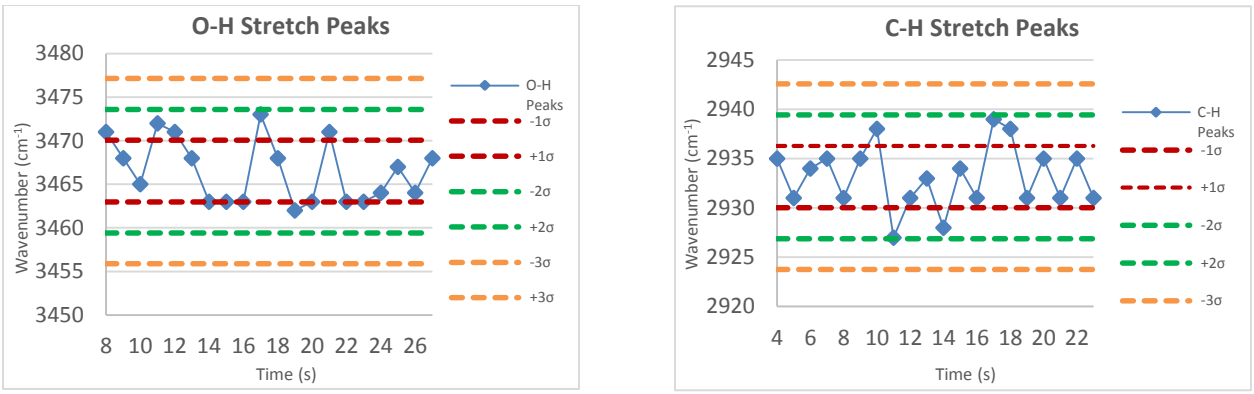

Figure 4.3.1: Organosolv lignin O-H stretch peaks (left) and C-H stretch peaks (right).

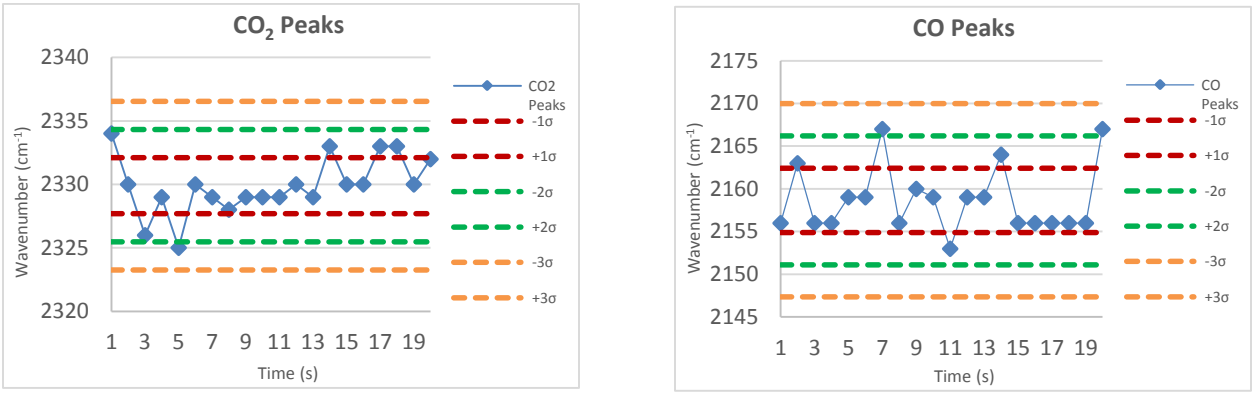

Figure 4.3.2: Organosolv lignin CO_2 peaks (left) and CO peaks (right).

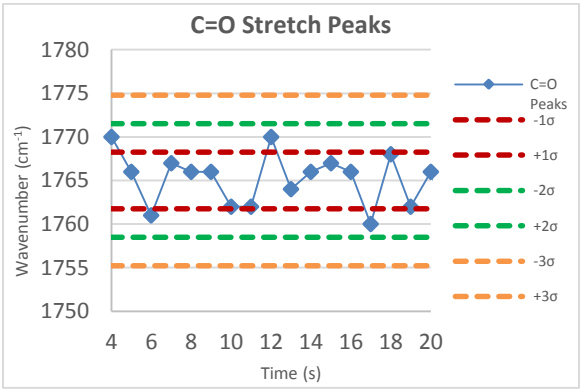

Figure 4.3.3: Organosolv lignin C=O stretch peaks.

According to organosolv lignin spectral evolution graph in Figure 4.2.6, peaks did not seem to shift over 1 s increments with the large wavenumber intervals on the x-axis of the graph.

However, one can observe in Figures 4.3.1-4.3.3 that peaks from different functional groups drift over time when analyzing with smaller intervals of wavenumber. Since peaks drift with respect to time, statistical analysis can be applied to determine what relevant window range is best to capture those data. Standard deviation (σ) was obtained for chosen peaks of different functional groups, and plotted in Figures 4.3.1-4.3.3. A conclusion can be drawn from the figures above, where 2 σ window range has the capability of capturing those data even when peaks drift over time. Although all peak points can be captured in window range of 3 σ, which is well within the window for analyses of time evolution of individual peaks reported herein. Hence, very little spectral shift is expected shift is expected. Similar results were obtained for pyrolyzed cellulose samples regarding the spectral shift of peaks over time. Data of selected peaks for pyrolyzed cellulose can be viewed in Appendix A.

4.4 Fumed Silca Lignin

As discussed in the previous sub-chapter, lignin is considered the most difficult to decompose due to the richness of aromatic rings and branches. The decomposition range of organosolv lignin varies from 100-900°C according to Yang et al. [45]. Therefore, a nominal particle size of 60 μm was used in this test in order to achieve higher heating rates during pyrolysis, where better yields of vapor products and volatiles can be obtained. Figure 4.4.1 displays a picture of pyrolyzed organosolv lignin after removal from the pyrolysis reactor. A large bubble shape is formed on the surface of the char due to the exothermic reaction during pyrolysis. An inference can be drawn that part of gas products and volatiles are trapped inside this char during pyrolysis. Therefore, another type of lignin (Fumed silica lignin) was introduced to investigate this phenomenon and allow for a higher wt% of gas products and volatiles to be produced.

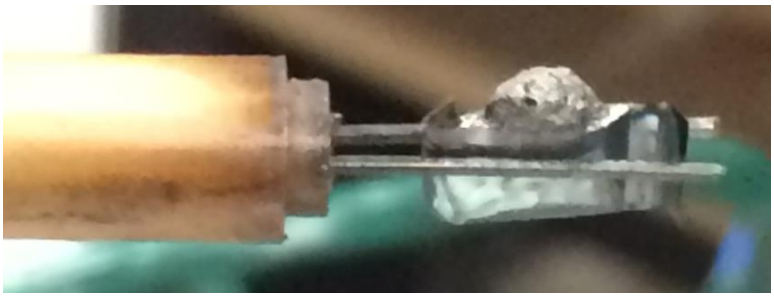

Figure 4.4.1: Picture of pyrolyzed organosolv lignin.

Fumed silica lignin is the mixture of solid heat carrier with organosolv lignin. The addition of solid heat carrier is to prevent agglomeration and improve heat transfer of lignin sample. The mixture was accomplished by blending the 1:1 ratio of organosolv lignin and filler with the help of solvent to promote homogeneity in the mixture. First, an appropriate amount of lignin derived from corn stover and filler (R974 hydrophobic fumed silica, Evonik) were combined in a glass beaker and mechanically mixed with a stirrer. Subsequently, the mixture was dispersed into 30mL of isopropyl alcohol as a solvent with the help of a sonicator for 15 minutes. Then, the suspension was placed in a vacuum oven at 40°C for 15 hours. Later, the finer powder was utilized in the pyrolysis test.

Figure 4.4.2: Pyrolyzed fumed silica lignin.

Pyrolyzed fumed silica lignin is displayed in Figure 4.4.2 in which powdery char is formed inside of the sample cup rather than the formation of the bubble shape. It is hypothesized that this lignin

type will allow larger wt% of vapor productions as well as volatiles since gas products able to completely release during pyrolysis . Evolution tests of these two lignin will be analyzed using a FTIR spectrometer and are discussed in the following sub-chapter.

4.5 Evolution Tests

The time evolution of specific functional groups for two types of lignin was analyzed during fast pyrolysis using the Agilent Resolution Pro software. This test provides a closer look at the evolution from chosen functional groups. The location of selected peaks was centered around 3570 cm^{-1} (OH stretch), 2920 cm^{-1} (C-H stretch), 2320 cm^{-1} (CO_2), 2150 cm^{-1} (CO), and 1750 cm^{-1} (C=O stretch). Mass samples of 3 mg, 5 mg and 7 mg were tested to gage the effects of mass loading on heat and mass transfer limitation. A sample mass of 7 mg would represent a thicker sample and therefore potentially more heat and mass transfer limitations. In the case of fumed silica lignin, these tests posed a challenge with regard to mass loading. This mixture had a ratio of 1:1 fumed silica and organosolv lignin; thus double the sample mass is required to match the mass of biomass. With a fixed dimension of the sample cup for the whole experiment, it was difficult for that large amount of sample to entirely fit inside. Moreover, weight loss occurred due to small amount of sample falling out of the sample cup during rapid insertion into the pyrolysis reactor. Measurements were made under two residence times to investigate differences that might appear in the early decomposition process. Once again, residence times used in this test are 0.38 s and 0.56 s. Both lignin samples are left inside the pyrolysis reactor for 55 seconds before removal.

Figure 4.5.1 provides profiles of gas products evolved from pyrolyzed organosolv lignin and fumed silica lignin. Both tests are performed with sample mass of 7 mg with a flow of 1 slpm heated nitrogen, which corresponds to a residence time of 0.56 s.

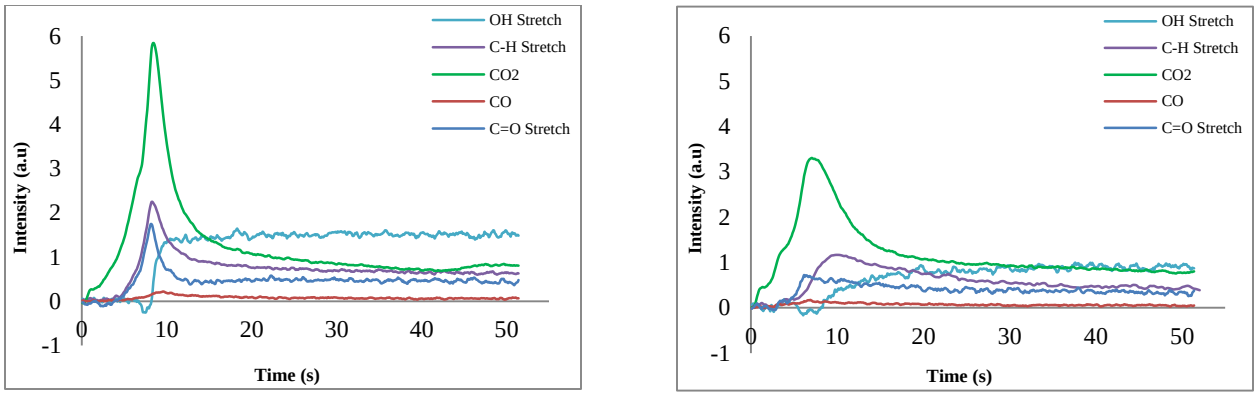

Figure 4.5.1: Evolution test of specific functional groups for organosolv lignin (left) and fumed silica lignin (right).

There is evidence that the functional groups are evolving differently during the pyrolysis reaction. The CO_2 signal for both lignin samples appear immediately after injection and reaches a plateau before rising again at about 1 s to a peak intensity at about 8 s. There is a second rise in the CO_2 profile for fumed silica lignin starting at 3.5 s when the sample holder is at about 467°C, and before the appearance of C=O stretch, C-H stretch, and CO functional groups. The vapor release of CO had the lowest absorption signal. According to Yang et al., a higher concentration of CO will only release at higher temperature (>600°C) [45]. Furthermore, the O-H stretch functional group for both lignin samples dips down to a negative intensity before starting to rise at time that is significantly delayed from other species. Furthermore, the pyrolysis of fumed silica lignin provided wider temporal peaks for functional groups of CO_2, C-H stretch and C=O stretch since gas products and volatile compounds are able to completely escape in the absence of the formation of chat bubble. However, the release of gas products for selected functional groups had a lower intensity in this case than for organosolv lignin. The following sub-chapter provides details about different sample mass loading for both lignin samples conducting at two residence times.

4.5.1 Sample Mass Analysis for O-H Stretch Functional Group

The gas evolution profiles of the O-H functional group from pyrolyzing organosolv lignin and fumed silica lignin at different mass loadings and residence times are plotted in Figures 4.5.2 and 4.5.3. Sample masses of 3 mg, 5 mg and 7 mg for both lignin samples are pyrolyzed with residence times of 0.38 s and 0.56 s. Different sample mass loadings are used to evaluate possible differences due to heat and mass limitations on the different initial reactions and biomass decomposition. The initial reactions of pyrolyzed lignin samples were plotted side by side for comparison with residence time, t_{res}, of 0.56 s and 0.38 s are plotted on the left and right respectively.

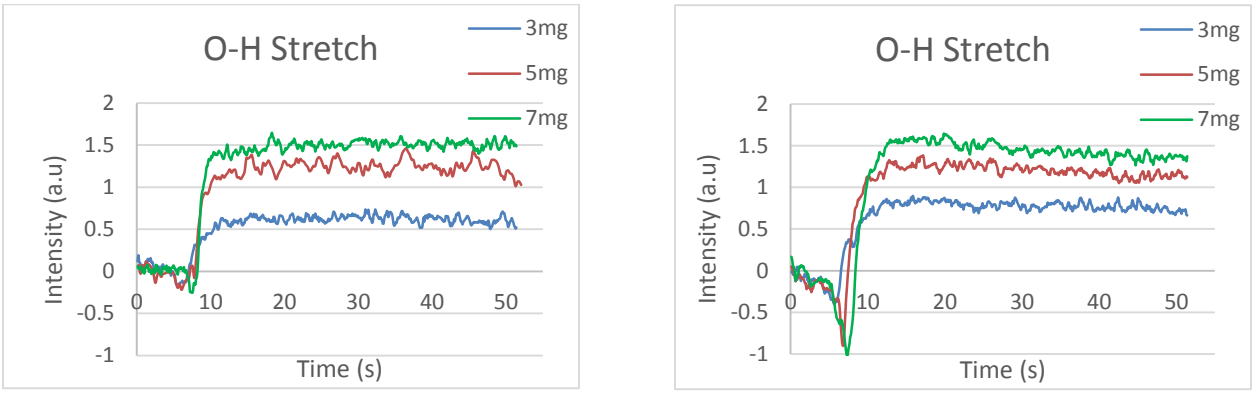

Figure 4.5.2: Organosolv lignin O-H stretch evolution with t_{res} of 0.56 s (left) and 0.38 s (right).

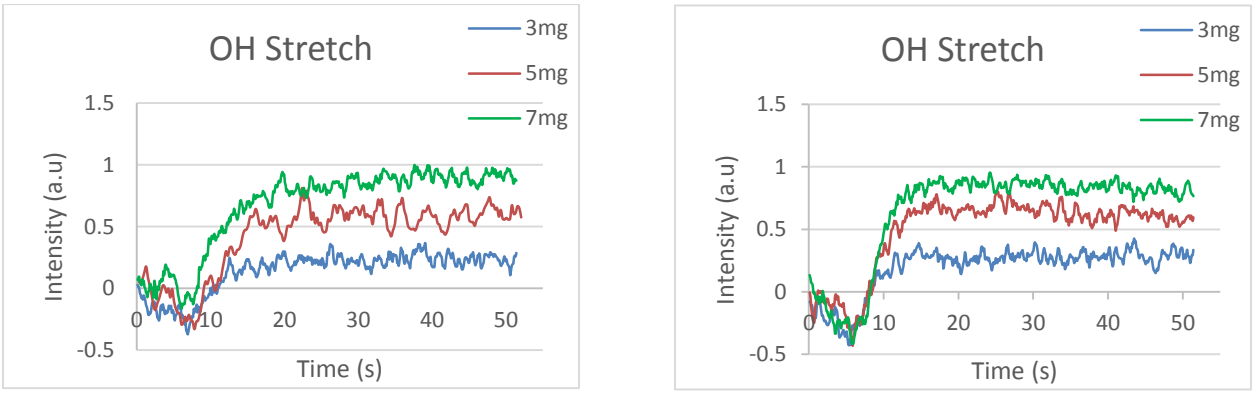

Figure 4.5.3: Fumed silica lignin O-H stretch evolution with t_{res} of 0.56 s (left) and 0.38 s (right).

It is interesting to note that the starting times of reaction are very similar for both the organosolv lignin and fumed silica lignin, However, the rate of rise of O-H stretch is faster for the case of organosolv lignin. This implies potential mass or heat transfer limitations for the case of fumed silica lignin. An anomaly can be observed where the O-H stretch functional group dips down below zero intensity before starting to rise at both residence times. Since the system is purged before every test and other species do not display the same dip signal as shown in Figure 4.5.1, it is possible that this dip is associated with residual water vapor in the system and problems with background subtraction. By comparison with organosolv lignin, lower intensity is achieved for fumed silica lignin with the same mass loading. The O-H absorption signal continues in the pyrolysis reactor until the removal of pyrolyzed samples. A possible explanation is that heated flow of nitrogen at the bottom of the reactor is low, and gas products with O-H stretch functional groups are unable to be carried out of the exhaust vent. This is consistent with the dip in the O-H signal discussed above.

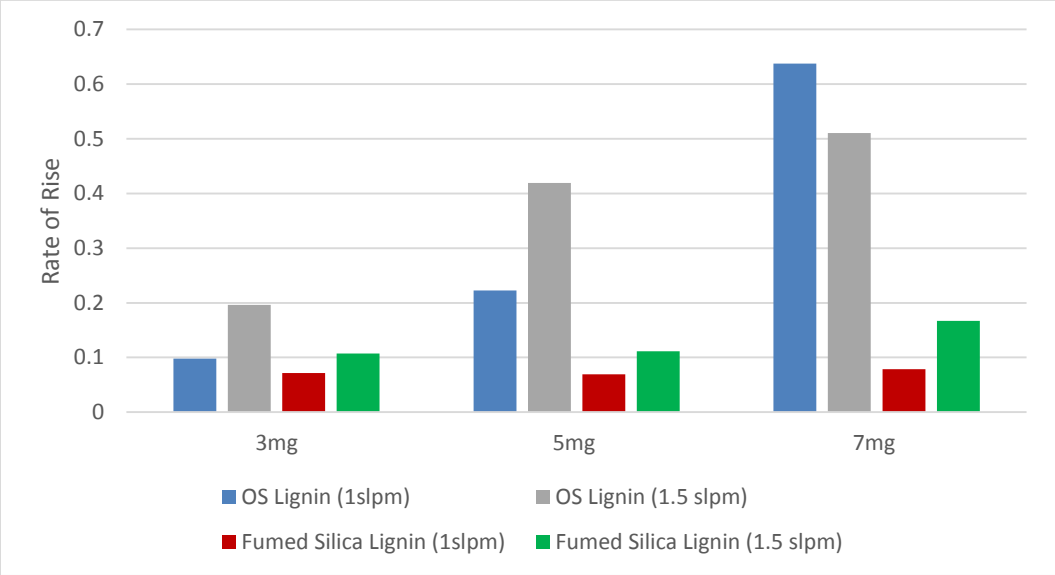

Figure 4.5.4: Rate of rise for O-H stretch functional group at 10-90% of peak intensity.

To obtain a numerical value for the rate of rise for different sample mass loadings, data in Figure 4.5.2 and 4.5.3 were further analyzed from 10-90% of their highest peak intensity with respect to time. These values are plotted in Figure 4.5.4. Although the O-H stretch functional group dips down below zero intensity for every sample mass loading, it is important to include those data when analyzing 10-90% rate of rise rather than selecting the initial data at zero intensity. Important data which fall below zero intensity will be missed if one only analyze data starting from zero intensity. In Figure 4.5.4, the rate of rise for two different lignin samples increases with the increase of sample mass loading. This implies that the increased mass loading does not sufficiently reduce the heating rate to reduce the rate of rise of the pyrolysis products.

A higher rise rate is generally achieved with shorter vapor residence time (0.38 s) of heated nitrogen flow due to biomass sample having a higher heating rate during pyrolysis. However, in the case of 7 mg for organosolv lignin, a higher rise rate is achieved at a longer residence time (0.56 s). This is due to longer intensity of O-H stretch over time, thus resulting in a lower rise rate. As an alternative to the 10-90% rise rate, a higher rise rate can be achieved with the used of smaller interval of window (such as 20-80%, 30-70%, and 40-60%). However, important data from the starting and ending reaction from the highest peak intensity will be missed.

4.5.2 Sample Mass Analysis for C-H Stretch Functional Group

Similarly, gas profiles of the C-H functional group for both lignin samples were extracted from the FTIR software for different sample mass loadings conducted in two residence times, t_{res}, of 0.56 s and 0.38 s and plotted in Figure 4.5.5 and 4.5.6. This gives an insight of how heat and mass transfer, as well as initial reactions affect the gas product of the C-H stretch from fast pyrolysis for both lignin samples.

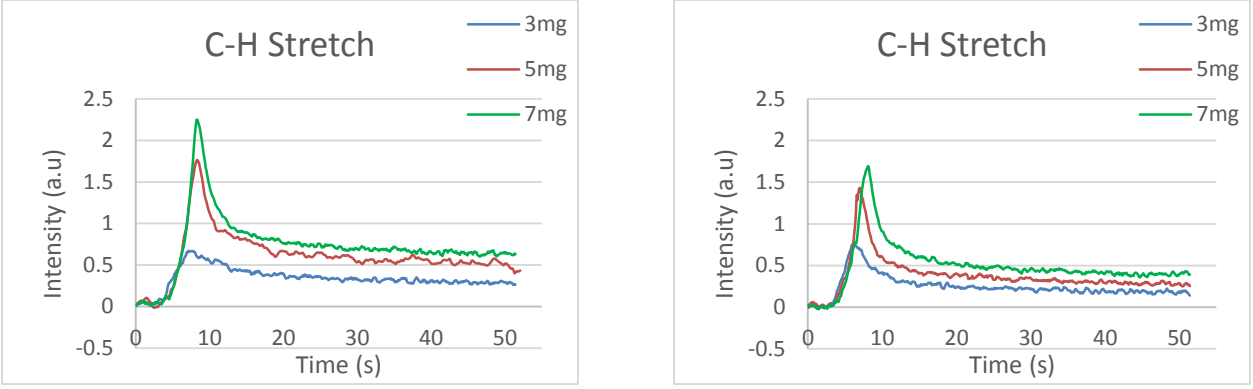

Figure 4.5.5: Organosolv lignin C-H stretch evolution with t_{res} of 0.56 s (left) and 0.38 s (right).

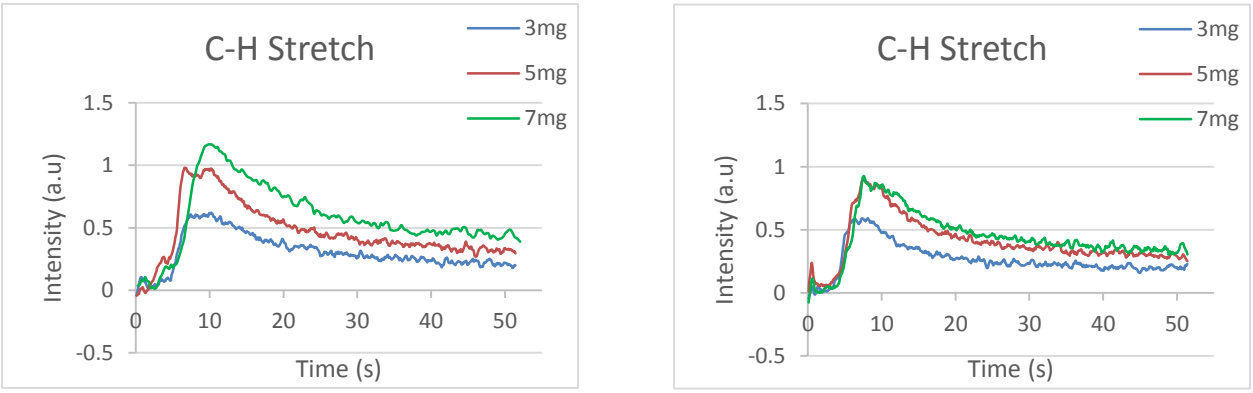

Figure 4.5.6: Fumed silica lignin C-H stretch evolution with t_{res} of 0.56 s (left) and 0.38 s (right).

Through evolution plots of C-H stretch functional group, one can observe that the release of this gas product occurs over longer periods of time with larger mass loading. This is due to heat or mass transfer limitations. Evolution plots are similar for both residence times, with longer residence time (left side of both Figures above) having higher intensity. It is believed that higher intensity of gas products will be achieved for biomass samples at a shorter residence time (0.38 s), however, it is not the case for the C-H stretch functional group. Comparing with organosolv lignin, fumes silica results in wider temporal peaks. In addition, the intensity signal is lower for fumed silica lignin, as was the case for O-H discussed earlier. Another observation is that two intensity peaks are formed for every mass loading conducted at different residence times. This issue might

be due to both lignin samples soaring off the sample cup from rapid insertion, allowing some lignin samples to decompose at the beginning of the reaction. Future work may consider modifying the sample holder to prevent biomass from falling out of the sample cup during insertion.

The rate of rise of the C-H stretch functional group for different sample mass loadings at two residence times can be analyzed from 10-90% of their highest peak intensity as shown in Figure 4.5.7.

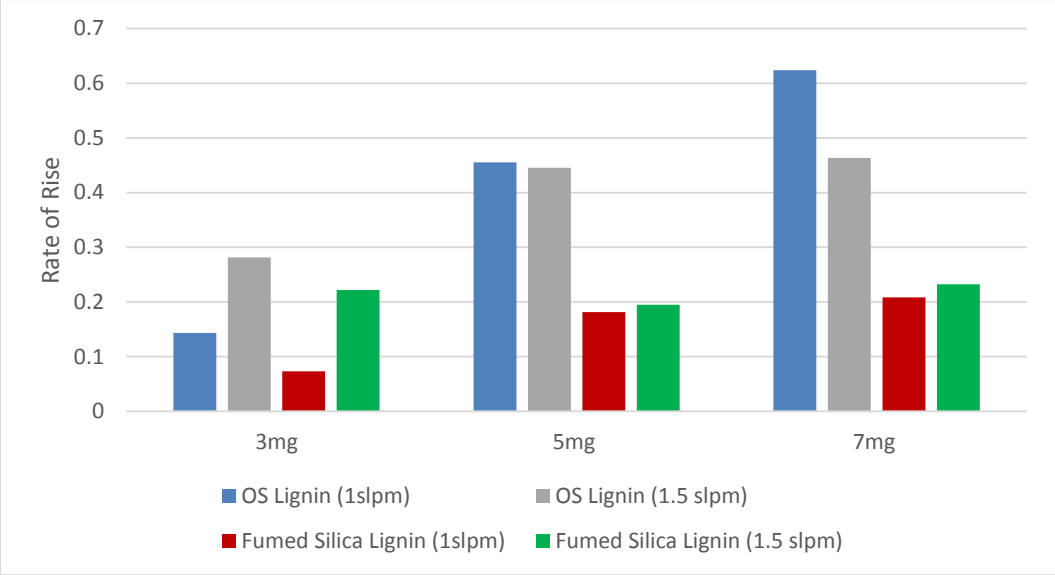

Figure 4.5.7: Rate of rise for C-H stretch functional group at 10-90% of peak intensity.

The reaction of C-H stretch functional group for both lignin samples begins around 3.5 s after being introduced into the preheated pyrolysis reactor. In Figure 4.5.7, one can observe that the rate of rise from 10-90% of their peak intensity increases with an increase of sample mass loadings. Since the plots for the C-H stretch functional group for every sample mass loading reaches the peak intensity in shorter time for organosolv lignin, as shown in Figure 4.5.5, the rise rate measured for both residence times is generally higher compared to fumed silica lignin. By comparing two different residence times for organosolv lignin, the rise rate for lower flow of

heated nitrogen is higher in the case of 5 mg and 7 mg. The rate of rise for fumed silica lignin is generally low for all sample mass loadings at two residence times. This is due to longer time is required for the C-H stretch functional group to reach the peak intensity.

4.5.3 Sample Mass Analysis for CO_2 Functional Group

Various branches of aromatic rings were found in lignin, leading to a wide range of temperatures to break down its chemical bonds [12,16]. By comparison with cellulose and red oak, it appears that lignin is considered the most difficult to decompose in pyrolysis. One solution to overcome this issue is by selecting a smaller particle size (<60 µm) for lignin so that a higher heating rate can be achieved during pyrolysis. Evolution graphs of CO_2 displayed in Figure 4.5.8 and 4.5.9 are the results of pyrolyzed lignin samples for 3mg, 5 mg, and 7 mg at two different residence times.

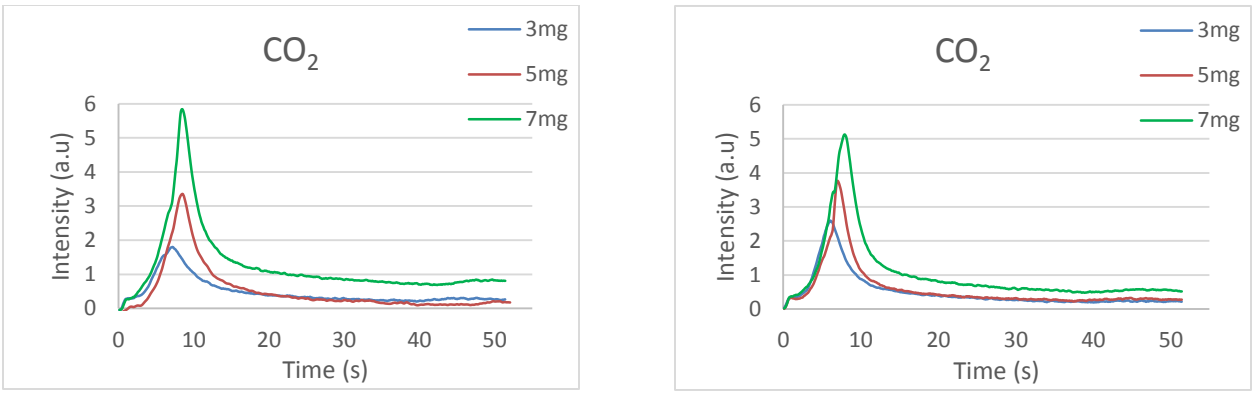

Figure 4.5.8: Organosolv lignin CO_2 evolution with t_{res} of 0.56 s (left) and 0.38 s (right).

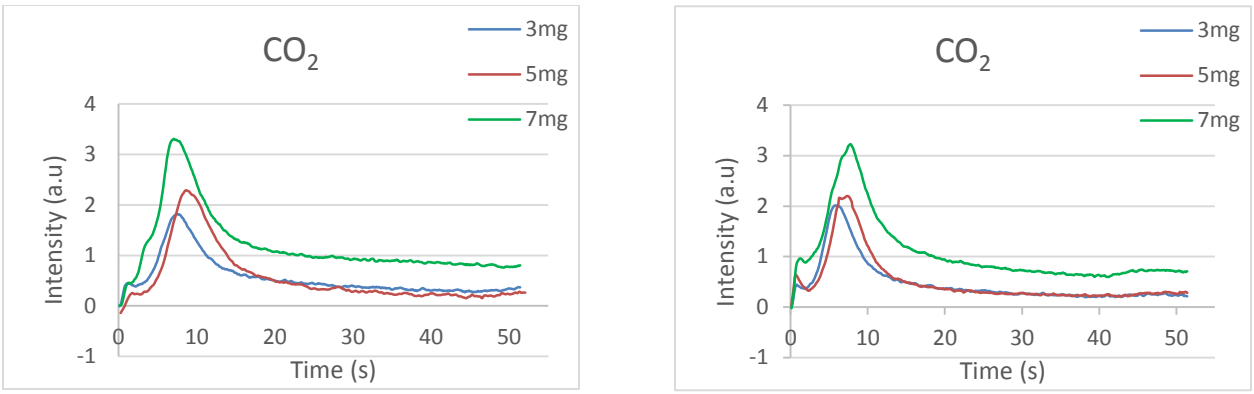

Figure 4.5.9: Fumed silica lignin CO_2 evolution with t_{res} of 0.56 s (left) and 0.38 s (right).

The gas release of CO_2 had the highest intensity and started to evolve at an early stage. With the development of this reactor, two intensity peaks are observed in the CO_2 spectrum, where the smaller peak appears immediately after injection, and the broader peak is found around 8 s when the sample holder is approximately at about 550°C for every sample mass loading. These plots are consistent for every sample mass loading and can be cleary seen for fumed silica lignin at both residence times. The first peak might be due to sample on the surface of both lignin samples started to pyrolyze radiately once it is introduced into the pyrolysis reactor which is preheated to 550°C environment. The latter peak occurred when the biomass sample achieved the same temperature as the sample cup. Another possibility is that some of the sample could have fallen off from the sample cup during rapid insertion, in which some samples start to decompose without the formation of other products. Also, much sharper and narrow peaks are formed in organosolv lignin for the evolution case of CO_2 at different sample mass loadings. A possible explanation for these sharp and narrow peaks is that this is due to gas product being trapped inside of the formation of char during pyrolysis, as shown in Figure 4.4.1, resulting in a rapid decrease from the peak.

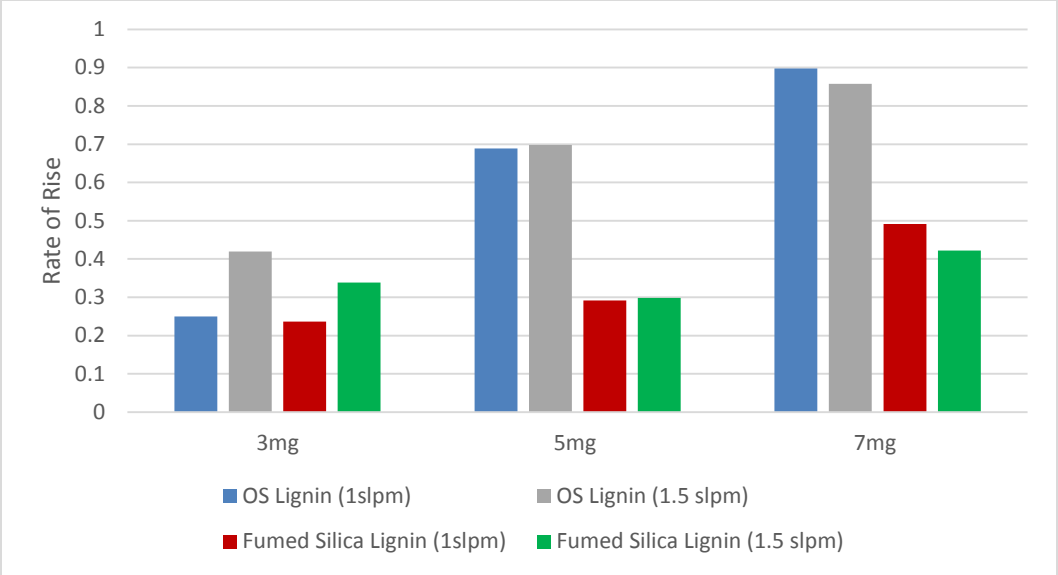

Figure 4.5.10: Rate of rise for CO_2 functional group at 10-90% of peak intensity.

Data on rise rate were plotted to show the rise of CO_2 intensity over time. Figure 4.5.10 shows the rate of rise for the CO_2 functional group taken from 10-90% of the highest peak intensity for all sample mass loadings at different residence times. Similar to both O-H stretch and C-H stretch functional groups, the rate of rise increases with an increase of sample mass loadings at different product residence times. It appears that the rise rate is significant for sample masses of 5 mg and 7 mg in the case of organosolv lignin at two residence times. Note that the intensity of the CO_2 signal is lower compared to organosolv lignin. Futhermore, longer time is required for the CO_2 functional group to reach the peak intensity in the case of fumed silica lignin. This results in low rise rate, particularly in the 5 mg sample at two vapor residence time.

4.5.4 Sample Mass Analysis for C=O Stretch Functional Group

Heat and mass transfer limitations were analyzed with sample masses of 3 mg, 5 mg, and 7 mg being inserted into the pyrolysis reactor at two different residence times. The evolution plots are shown in Figures 4.5.10 and 4.5.11. A high sampling speed of 75 kHz together with a resolution

of 8 cm^{-1} were selected to obtain reliable trends for comparison. The time resolution for this test is fixed at 0.106 seconds based on the analytical software.

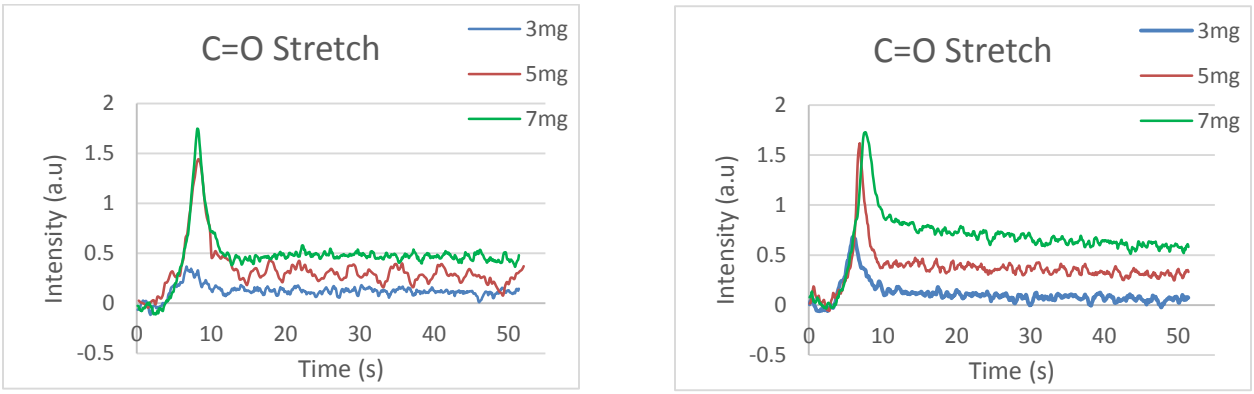

Figure 4.5.11: Organosolv lignin C=O stretch evolution with t_{res} of 0.56 s (left) and 0.38 s (right).

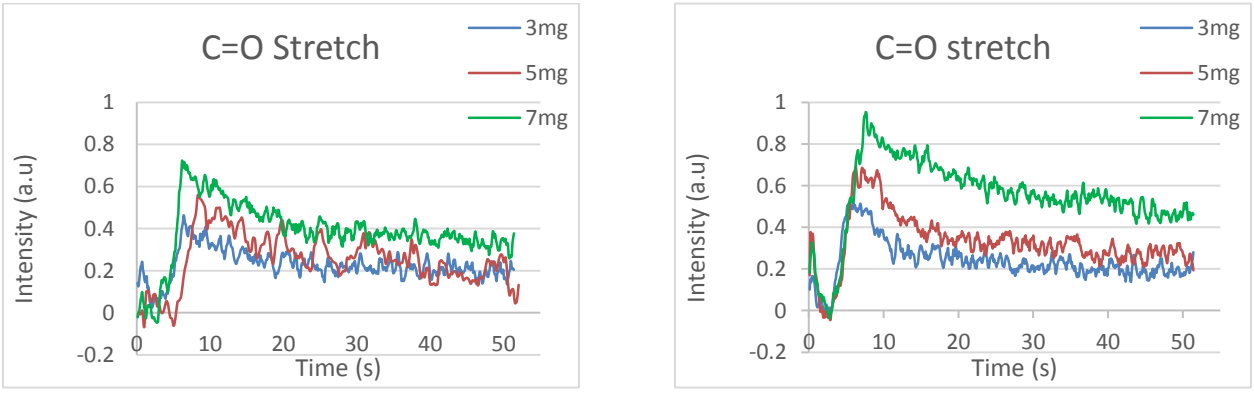

Figure 4.5.12: Organosolv lignin C=O stretch evolution with t_{res} of 0.56 s (left) and 0.38 s (right).

The intensity of the C=O stretch functional group achieved the third highest intensity after CO_2 and C-H stretch. The starting time of the reactions and the rate at which signal rise are similar for all mass loadings when comparing C=O stretch bond group except for the case of fumed silica at longer residence (0.56 s). The reaction of the C=O stretch functional group begins around 3 s for both lignin samples at a sample cup temperature of 460°C. A similar trend of sharper and narrow peaks can be observed for organosolv lignin at different sample mass loadings due potentially to gas product trapped inside the formation of char during fast pyrolysis. Intensity

signal for all sample mass loadings at two residence time did not appear to fall to zero intensity after being pyrolyzed for 55 s in the reactor. This is due to low flow of heated nitrogen being unable to sweep the gas products out of the reactor.

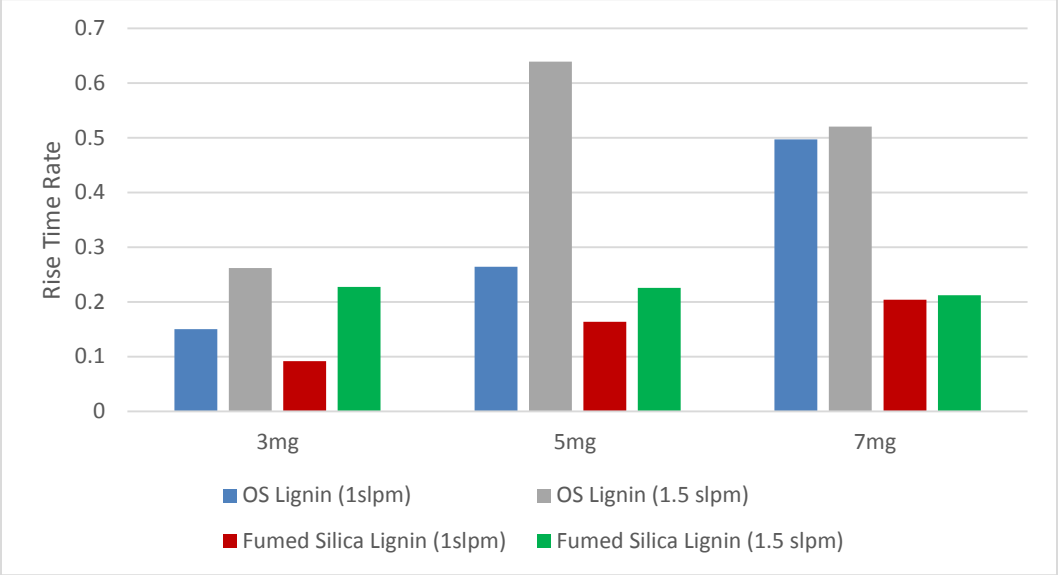

Figure 4.5.13: Rate of rise for C=O stretch functional group at 10-90% of peak intensity.

The rates of rise for the C=O stretch functional group were further analyzed from 10-90% of their highest peak intensity and plotted in Figure 4.5.12. A higher rise rate is achieved with the increase of sample mass and residence time for both lignin samples. A significant rate of rise can be observed for 5 mg of organosolv lignin at a shorter residence time (0.38 s). In Figure 4.5.11, fumed silica lignin produced a wider temporal peak compared to organosolv lignin, yet the intensity is low. Since powdery char is formed inside the sample cup after fumed silica lignin being pyrolyzed, there is a possibility that this lignin sample is not fully pyrolyzed. Similarly, longer time is required for the gas product of C=O stretch of fumed silica lignin to reach their highest peak intensity, resulting in a low rate of rise for both residence times.

The release of CO for both lignin samples had the lowest absorpbtion signal among selected functional groups. According to Yang et al., the production of CO is less for lignin at lower temperatures because CO is released primarily at temperatures of 760°C due to secondary reactions [50]. Since the intensity of selected function groups has been reduced, the CO signal is very low for fumed silica lignin. The evolution plots of CO for both lignin samples are presented in Appendix C. Data of 10-90% rate of rise for CO were not able to be determined because of substantial noise occurring in the plot for all mass loadings.

It is interesting to note that the signal for organosolv lignin is consistently higher by about a factor of two compared with fumed silica lignin for the different functional groups and flow conditions. This provides some confidence as to the repeatability of measurements and usefulness for qualitative comparison between different conditions. The rate of rise also showed consistent trends, with the rise rate of products being faster for the case of organosolv lignin. Hence, the FTIR instrument is shown to be a reasonable device for capturing the time dynamics of product formation during fast pyrolysis.

CHAPTER 5. CONCLUSIONS AND RECOMMENDATIONS

5.1 General Conclusions

The purpose of this project is to develop an optically accessible, bench-scale fast pyrolysis reactor to allow time-resolved analysis of the fast pyrolysis reaction process. A bench-scale fast pyrolysis reactor with high temperature and optical access capabilities was developed to study the *in-situ* time evolution of the reactions of various biomass feedstocks using a FTIR analytical instrument. A compartment was machined to successfully insert samples into the pyrolysis reactor. In order to produce consistent results for each experimental run, a custom-built, automated sample insertion mechanism was developed to allow rapid insertion of biomass feedstock into the heated environment by applying a fixed voltage onto a solenoid driver. Fourier Transform Infrared (FTIR) Spectroscopy was used to analyze the temporal evolution of products with the ability to differentiate parts of the FTIR spectrum. Due to the pyrolysis reactor being unable to fit internally into the FTIR sample compartment, modifications were made by taking the signal beam out of the FTIR commercial instrument to pass through the reactor. Although the identification of individual compounds is challenging, the FTIR analytical instrument can provide information on bonding from molecular vibrations for analysis of functional groups. Biomass feedstock of organosolv lignin and fumed silica lignin were selected for demonstration measurements. Three separate sample mass loadings of 3 mg, 5 mg, and 7 mg were utilized with two product residence times (0.38 seconds and 0.56 seconds). Analysis of heat and mass transfer effects were performed using different sample mass loadings, while initial reactions could be studied at a different product residence times. Statistical analysis is applied to the spectrum for both lignin samples to determine that the effects of any spectra shift would be minimal in these experiments. Lastly, data on the rate

of rise for the evolution of both lignin samples were analyzed from 10-90% of their highest peak intensity.

Through the observation of evolution for organosolv lignin, it can be concluded that the release of CO_2 evolved at the very beginning, followed by C=O stretch then C-H stretch. The functional group of O-H stretch is the last to evolve for all cases. A large bubble shape of char was formed during the pyrolysis of organosolv lignin from corn stover, with products and volatiles seemingly being trapped within the solid phase. Hence, sharp and narrow peaks were observed from evolution graphs of selected organosolv lignin functional groups. Fumed silica lignin was introduced to overcome this issue where it shows significant differences with the organosolv lignin temporal evolution for all functional groups. Broader peaks can be observed in the evolution plot when fumed silica lignin is pyrolyzed.

5.2 Recommendations

The objective of this experiment was to develop a bench-scale fast pyrolysis reactor with optical access for *in-situ* analysis of fast pyrolysis for different biomass samples using FTIR spectroscopy. Initial reactions were analyzed during fast pyrolysis. However, further improvements can be made to the current cell design. It appears that a small part of the sample can fall out of the sample cup even before entering the pyrolysis reactor due to strong collision of the solenoid driver and the arm used for insertion of biomass samples. Springs can be installed onto the automated insertion mechanism to reduce vibration. Another suggestion would be making an automated plug for the sample insertion compartment on the reactor to prevent heated nitrogen from flowing out before every experimental run. A steel foil of thickness less than 25 microns can be used for the sample cup to further improve the heat transfer to biomass samples. Since the temperature of the sample holder may not represent the temperature of the sample itself, it would

be good to model this heat transfer process to predict the temperature rise within the sample for a given temperature rise of the sample holder.

To reduce experimental uncertainty, additional runs of various samples should be conducted to further evaluate consistency, repeatability as well as confidence. Furthermore, a more precise weight measurement of biomass feedstock should be used to obtain a more accurate result. Since biomass feedstock has a very complex mixture of compounds, a simpler compound such as phenol, guaiacol or levoglucosen can also be tested in this pyrolysis reactor where comparison of spectra can be made with the whole biomass feedstock to further differentiate products as well as study the time evolution of the products formation process. While this study demonstrated that the unique reactor design with optical access coupled with FTIR technique can provide new information about time-resolved reaction mechanism of fast pyrolysis, the combination with other experimental techniques should also be considered in order to provide a more accurate identification and qualification of the pyrolyzed biomass samples.

REFERENCES

[1] Department of Energy & Climate Change, "*DECC Fossil Fuel Price Projections"*. 2014

[2] U.S. Department of Energy, "*Alternative Fuels Data Center"*. 2014

[3] Suttibak S., Sriprateep K., and Pattiya A., "*Production of Bio-oil via Fast Pyrolysis of Cassava Rhizome in a Fluidised-Bed Reactor"*. Energy Procedia, Vol. 14, p. 668-673, 2012.

[4] Scott, D.S. and J. Piskorz, "*The Flash Pyrolysis of Aspen-polar wood"*. Canadian Journal of Chemical Engineering, Vol 60(5): p. 666-6741982

[5] Environmental and Energy Study Institute (EESI), "*Bioenergy (Biofuels and Biomass)"*. 2014

[6] Donald L. Klass, "*Biomass for Renewable Energy, Fuels, and Chemicals"*. Elsevier Inc, 1998

[7] Dimitriu S., "*Polysaccharides: Structural Diversity and Functional Versatility, Second Edition"*. Marcel Dekker, New York, 2005

[8] Hangarter R., "*Ecological Plant Physiology: Plant Cell Walls-a multilatered structure unique to plants"*.

[9] McKendry P., "*Energy production from biomass (part 1): overview of biomass".* Bioresource Technology. 83 (1), p. 37-46, 2002.

[10] Murphy J. D., and McCarthy K., "*Ethanol production from energy crops and wastes for use as a transport fuel in Ireland"*. Applied Energy, Vol. 82 (2), P. 148-166, 2005.

[11] Ophardt C. E., *Virtual Chembook: "Cellulose"*. 2003

[12] Mohan D., Pittman C. U., and Steele P.H., "*Pyrolysis of Wood/Biomass for Bio-Oil: A Critical Review*". Energy Fuels, Vol. 20(3), p.848-889, 2006.

[13] Harmsen P. F. H., Huijgen W.J.J, Lopez L. M. B., and Bakker R. R. C., Literature Review of Physical and Chemical Pretreatment Processes for Lignocellulosic Biomass. 2010.

[14] Wild P., Reith H., and Heeres E., "*Biomass pyrolysis for chemicals*". Biofuels, Vol. 2 (2), pp. 185-208, 2011.

[15] Pushkaraj R. Patwardhan, Robert C.Brown, Brent H. Shanks, "*Product Distribution from the Fast Pyrolysis of Hemicellulose*". ChemSusChem, Vol.4(5), p. 636-643, 2011.

[16] Dr. Samy Sadak, "*Pyrolysis*",http://bioweb.sungrant.org/NR/rdonlyres/57BCB4D0-1F59-4BC3-A4DD-4B72E9A3DA30/0/Pyrolysis.pdf, p. 1-24.

[17] Renewable Energy World, "*Biopower*". http://www.renewableenergyworld.com/rea/tech/bioenergy/biopower. 2015.

[18] Leo Aloysius W., "*The Mechanisms of Pyrolysis, Oxidation, and Burning of Organic Materials*". National Bureau of Standards Special Publication 357, 1972.

[19] F. Shafizadeh, "*Introduction to Pyrolysis of Biomass*". Journal of Analytical and Applied Pyrolysis, Vol. 3, pp. 283-305, 1982.

[20] Robert J. Evans, Thomas A. Milne, "*Molecular characterization of the pyrolysis of biomass*". Energy Fuels, Vol. 1 (2), pp. 123-137, 1987.

[21] M. C. Blanco Lopez, C. G. Blanco, A. Martinez-Alonso, J. M. D. Tascon, "*Composition of gases released during olive stones pyrolysis*". Journal of Analytical and Applied Pyrolysis, Vol. 65, pp. 313-322, 2002.

[22] Philipp Morf, Philipp Hasler, Thomas Nussbaumer, "*Mechanisms and kinetics of homogenous secondary reactions of tar from continuos pyrolysis of wood chips*". Fuel, Vol. 81, pp. 843-853, 2002.

[23] Sevgi Sensoz, "*Slow Pyrolysis of wood barks from Pinus brutia Ten. And product compositions*". Bioresource Technology, Vol. 89 (3-89), p. 307-311, 2003

[24] Paul T. Williams, Serpil Besler, "*The influence of temperature and heating rate on the slow pyrolysis of biomass*". Renewable Energy, Vol. 7 (3), pp. 233-250, 1996.

[25] A V. Bridgwater, D. Meier, D. Radlein, " *An overview of fast pyrolysis of biomass*". Organic Geochemistry, Vol. 30, pp. 1479-1493, 1999.

[26] A. V. Bridgwater, " *Review of fast pyrolysis of biomass and product upgrading*". Biomass and Bioenergy, Vol. 38, pp. 68-94, 2012.

[27] Roberto Aguado, Martin Olazar, Beatriz Gaisan, Ruben Prieto, Javier Bilbia, "*Kinetic Study of Polyolefin Pyrolysis in a conical Spouted Bed Reactor*". Ind. Eng. Chem. Res., Vol. 41 (18), pp. 4559-4566, 2002.

[28] T. Cornellissen, J. Yperman, G. Reggers, S. Schreurs, R. Carleer, "*Flash co-pyrolysis of biomass with polyactic acid. Part 1: Influence on bio-oil yield and heating value*". Fuel, Vol. 87 (7), pp. 1031-1041, 2008.

[29] A. V. Bridgwater, " *Renewable fuels and chemicals by thermal processing of biomass*". Chemical Engineering Journal, Vol.91, pp. 87-102, 2003.

[30] A. V. Bridgwater, " *Principles and practice of biomass fast pyrolusis processes for liquids*". Journal of Analytical and Applied Pyrolysis, Vol.51 (1), pp. 3-22, 1999.

[31] C. Dupont, J. M. Commandre, P. Gauthier, G. Boissonnet, S. Salvadoe, D. Schweich, " *Biomass pyrolysis experiments in an analytical entrained flow reactor between 1073 K and 1273 K*". Fuel, Vol.87 (7), pp. 1155-1164, 2008.

[32] M. K. Bahng, C. Mukarakate, D. J. Robinchaud, M. R. Nimlos, " *Current technologies for analysis of biomass thermochemical processing: A review*". Nalytica Chimica Acta, Vol. 651 (2), pp. 117-138, 2009.

[33] Dominguez A., Menendez J. A., Inguanzo M., Pis J. J., " *Production of biofuels by high temperature pyrolysis of sewage sludge using conventional and microwave heating"*. Bioresourse Technology, Vol.97(10), pp. 1185-1193, 2006.

[34] Juan A. Conesa, Rafael Font,Antonio Marcilla, Angela N. Garcia, "*Pyrolysis of Polyethylene in a Fluidized Bed Reactor*". Energy & Fuels, Vol. 8, pp. 1238-1246, 1994.

[35] A. V. Bridgwater, G. V. C. Peacocke, "*Fast Pyrolysis processes for biomass*", Renewable and Sustainable Energy Review, Vol. 4, pp 1-73, 2000.

[36] A. S. Chaurasia, B. V. Babu "*Modelling & Simulation of Pyrolysis of Biomass: Effect of Thermal Conductivity, Reactor Temperature and Particle Size on Product Concentration*".

[37] Jacques Lede, "*Biomass Pyrolysis: Comments on Some Sources of Condusion in the Definations of Temperature and Heating Rates*". Energy & Fuels, Vol. 3, pp. 886-898, 2010.

[38] Elly Hoekstra, Kees J. A. Hogendoorn, Xiaoquan Wang, Roel J. M. Westerhof, Sascha R. A. Kersten, Wim P. M. van Swaaij, Michiel J. Groeneveld, "*Fast Pyrolysis of Biomass in a Fludized Bed Reactor: In Situ Filtering of the Vapors*". Ind. Eng. Chem. Res., Vol. 48 (10), pp. 4744-4756, 2009.

[39] Pankaj K. Kanaujia, Y. K. Sharma, M. O. Garg, Deependra Tripathi, Raghuvir Singh, "*Review of analytical strategies in the production and upgrading of bio-oils derived*

from lignocellulosic biomass". Journal of Analytical and Applied Pyrolysis, Vol. 105, pp. 55-74, 2014.

[40] A. Oasmaa, E. Kuoppala, "*Fast Pyrolysis of Forestry Residue. 3. Storage Stability of Liquid Fuel*". Energy Fuels, Vol. 17 (4), pp. 1075-1084, 2003.

[41] Barbara Stuart, "*Infrared Spectroscopy: Fundamentals and Applications*". Wiley, 2004

[42] Koichi Nishikida, Etsuo Nishio, Robert W. Hannah, "*Selected applications of modern FT-IT Techniques*", Kodansha, 1995

[43] Peter R. Griffiths, James A. de Haseth, "*Fourier Transform Infrared Spectrometry*". Wiley, 1986

[44] M. W. Mackenzie, "*Advances in Pllied Fourier Transform Infrared Spectroscopy*". Wiley, 1988

[45] Haiping Yang, Rong Yan, Hanping Chen, Dong Ho Lee, Chuguang Zheng, "*Characteristics of hemicellulose, cellulose and lignin pyrolysis*". Fuel, Vol. 86, pp. 1781-1788, 2007.

[46] Peng Fu, Song Hu, Jun Xiang, Peisheng Li, Dan Huang, Long Jiang, Anchao Zhang, Junying Zhang, "*FTIR study of pyrolysis products evolving from typical agricultural residues*". Journal of Analytical and Applied Pyrolysis, Vol. 88 (2), pp. 117-123, 2010.

[47] C. Lievens, R. Carleer, T. Cornelissen, J. Yperman, "*Fast pyrolysis of heavy metal contaminated willow: Influence of the plant part*". Fuel, Vol. 88 (8), pp. 1417-1425, 2009.

[48] S. Li, J Lyons-Hart, J. Banyasz, K. Shafer, "*Real-time evoled gas analysis by FTIR method: an experimental study of cellulose pyrolysis*". Fuel, Vol. 80 (12), pp. 1809-1817, 2001.

[49] R.Bassilakis, R.M Carangelo, M.A Wojitowicz, *"TG-FTIR analysis of biomass pyrolysis"*. Fuel, Vol. 80 (12), pp. 1765-1786, 2001.

[50] R. Vinu and Linda J. Broadbelt, "A mechanistic model of fast pyrolysis pf glucose-based carbohydrates to predit bio-oil composition". Energy and Environmental Science, Vol. 5 (12), pp. 9808-9826, 2012.

[51] Q.Liu, S.Wang, Y. Zheng, A.Luo, K. Cen, "Mechanism study of wood lignin pyrolysis by using TG-FTIR analysis". Journal of Analytical and Applied Pyrolysis, Vol. 82, pp. 170-177, 2008

APPENDIX A. CELLULOSE SPECTRA PEAKS PLOTS

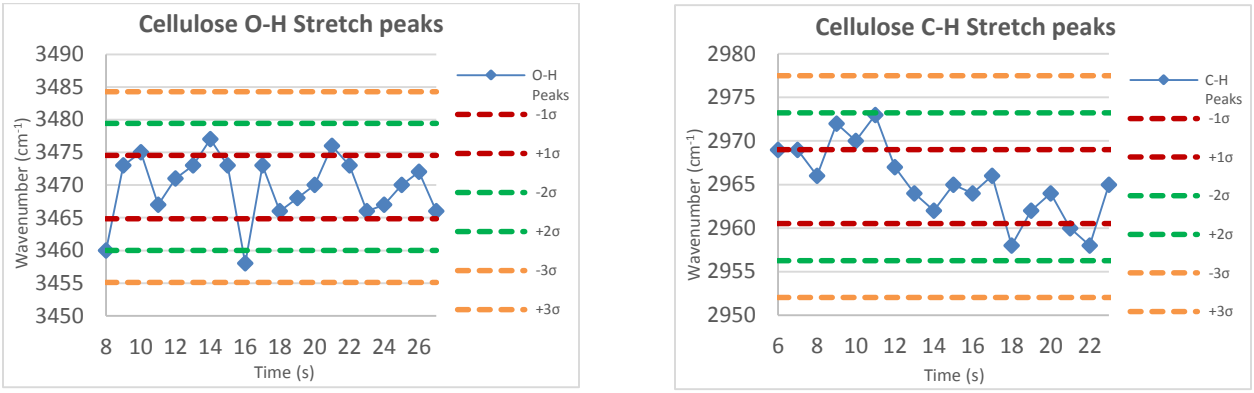

Figure A.1: Cellulose O-H stretch peaks (left) and C-H stretch peaks (right).

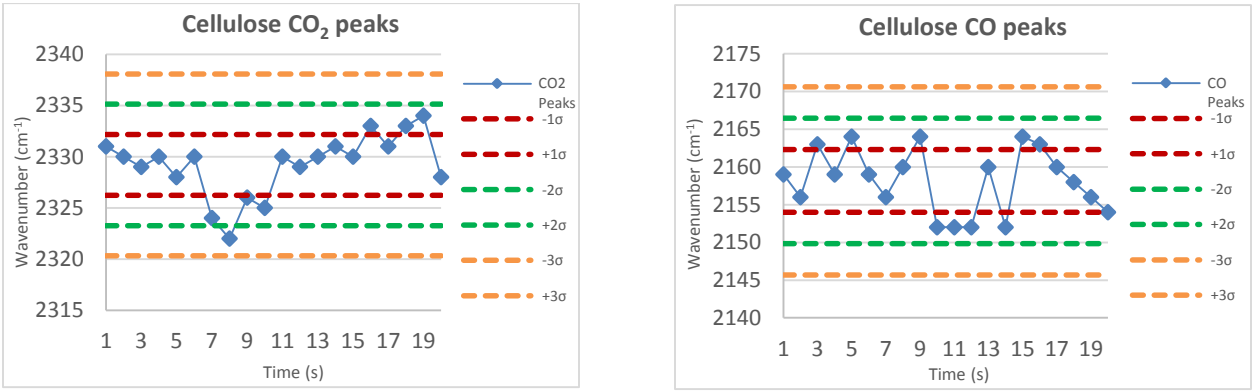

Figure A.2: Cellulose CO_2 peaks (left) and CO peaks (right).

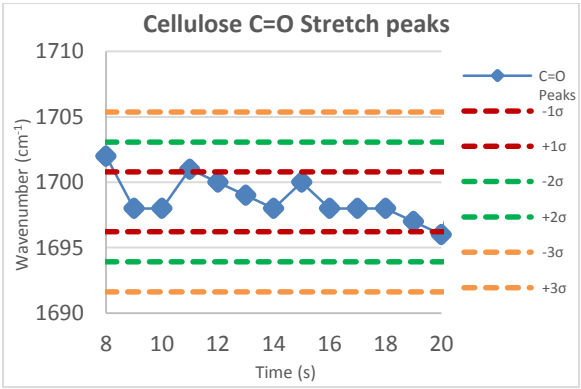

Figure A.3: Cellulose C=O stretch peaks

APPENDIX B. LIGNIN SAMPLES OF CO FUNCTIONAL GROUP PLOTS

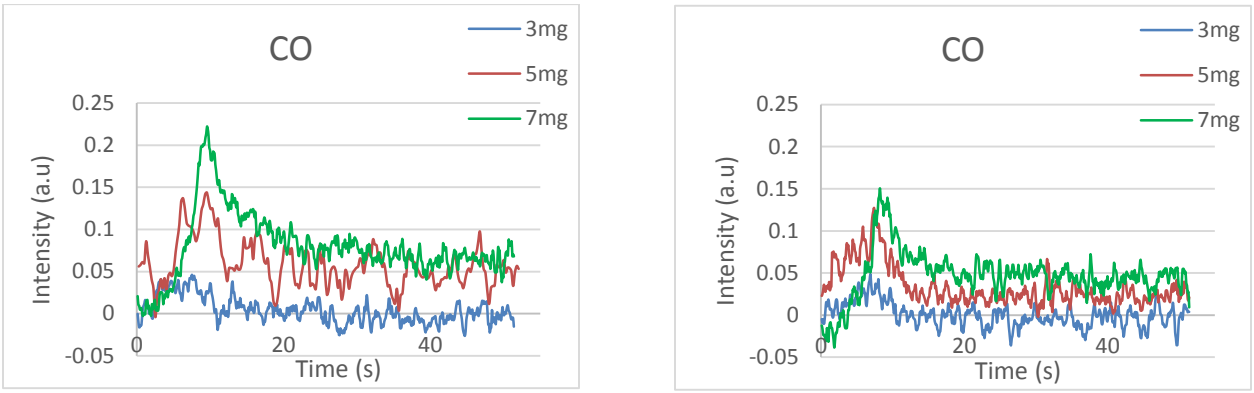

Figure B.1: Organosolv lignin CO evolution with t_{res} of 0.56 s (left) and 0.38 s (right).

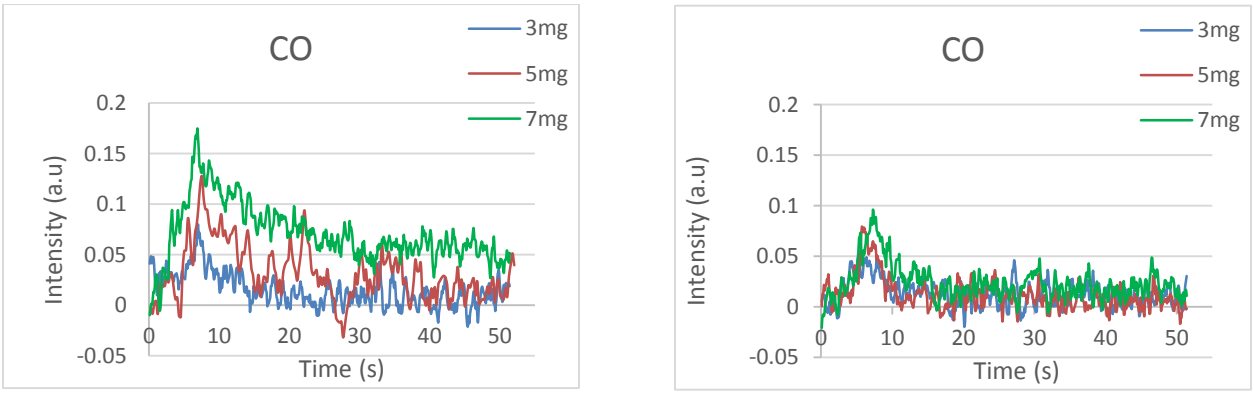

Figure B.2: Fumed silica lignin CO evolution with t_{res} of 0.56 s (left) and 0.38 s (right).

APPENDIX C. EVOLUTION TEST PLOTS

Below are the evolution plots for 7 mg of red oak and cellulose conducting at lower flow rate of heated nitrogen, which corresponds to a residence time of 0.56 s.

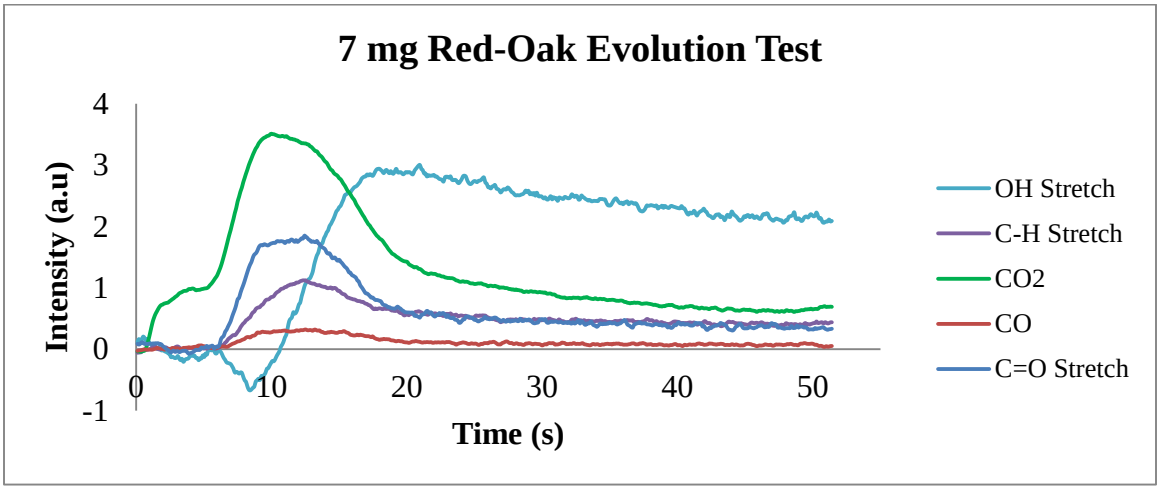

Figure C.1 Red-oak evolution test of specific functional groups.

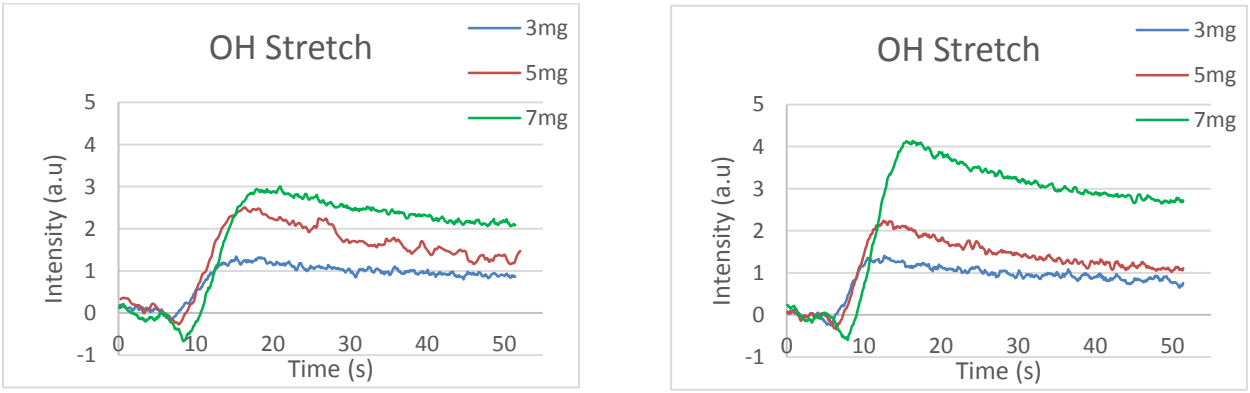

Figure C.1.1: Red-oak O-H stretch evolution with t_{res} of 0.56 s (left) and 0.38 s (right).

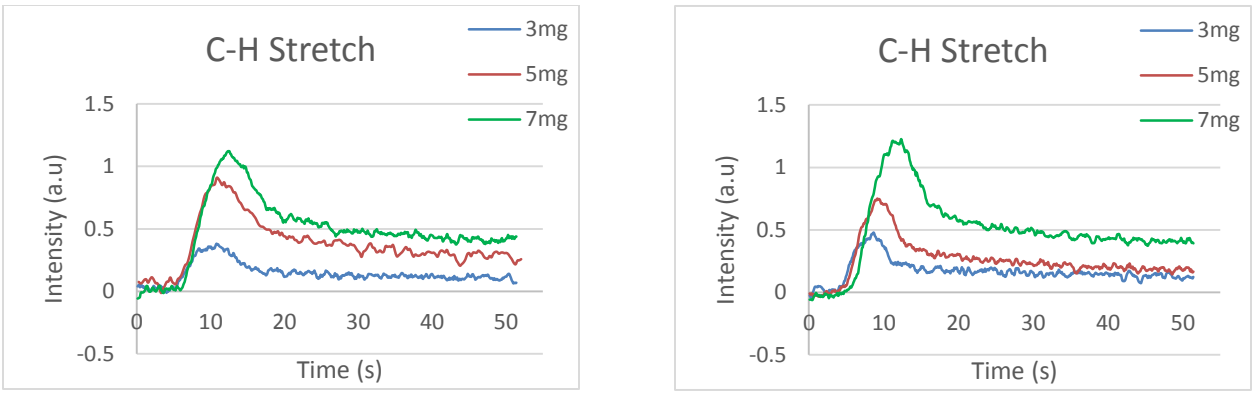

Figure C.1.2: Red-oak C-H stretch evolution with t_{res} of 0.56 s (left) and 0.38 s (right).

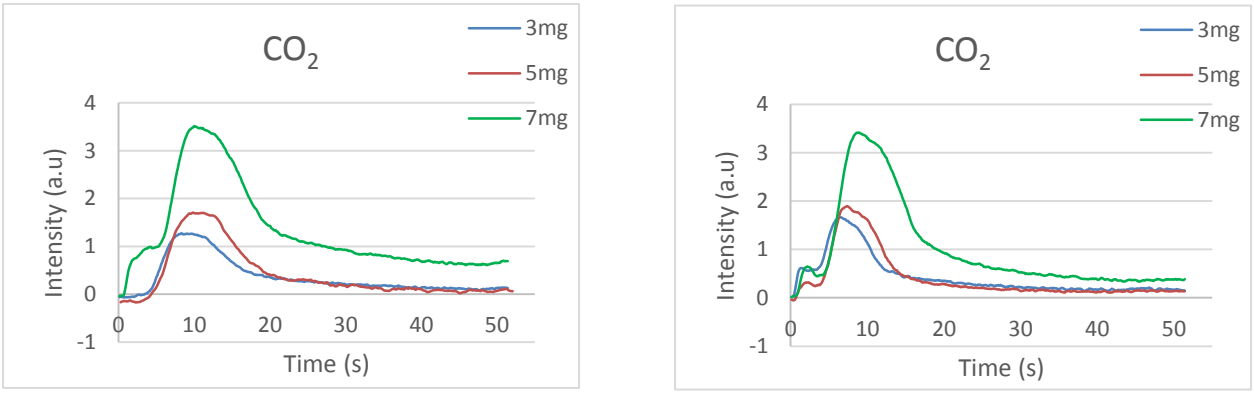

Figure C.1.3: Red-oak CO_2 stretch evolution with t_{res} of 0.56 s (left) and 0.38 s (right).

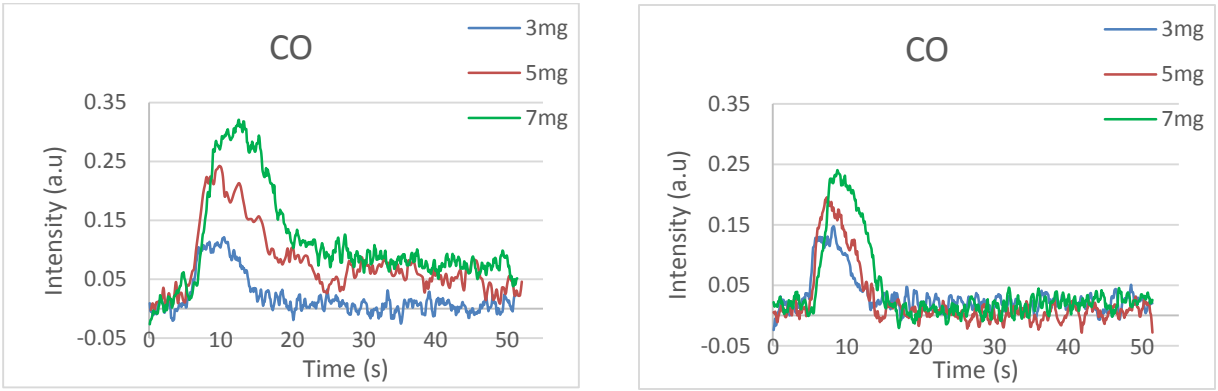

Figure C.1.4: Red-oak CO stretch evolution with t_{res} of 0.56 s (left) and 0.38 s (right).

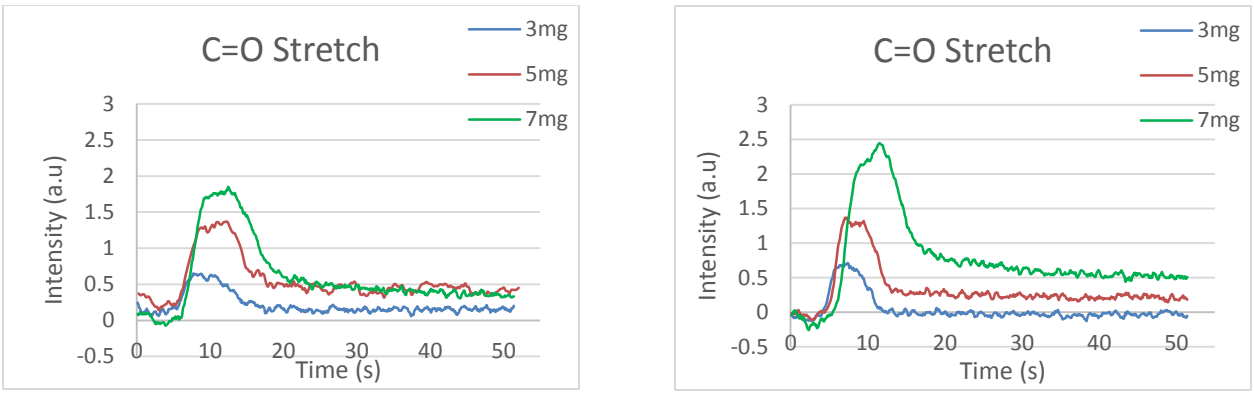

Figure C.1.5: Red-oak C=O stretch evolution with t_{res} of 0.56 s (left) and 0.38 s (right).

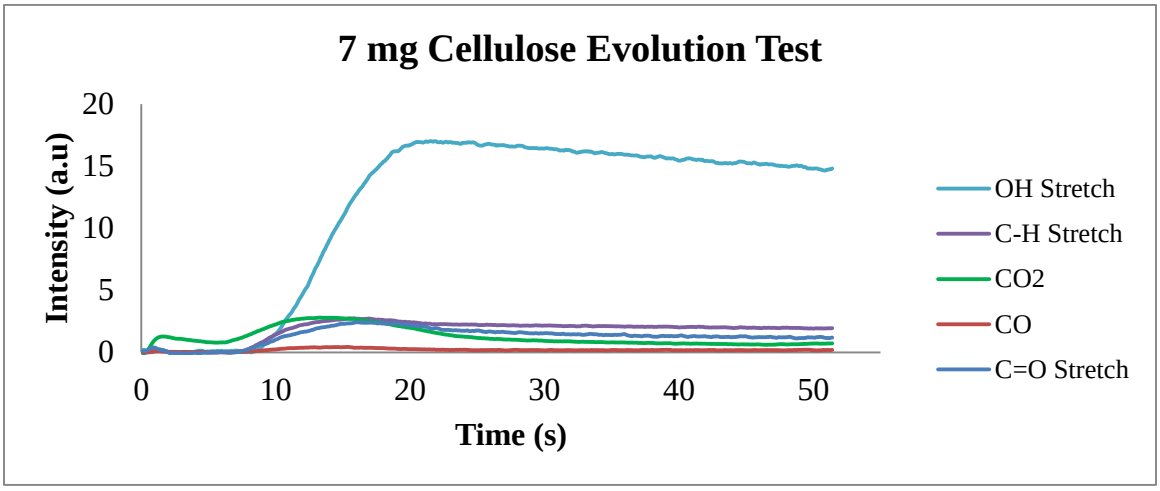

Figure C.2: Cellulose evolution test of specific functional groups.

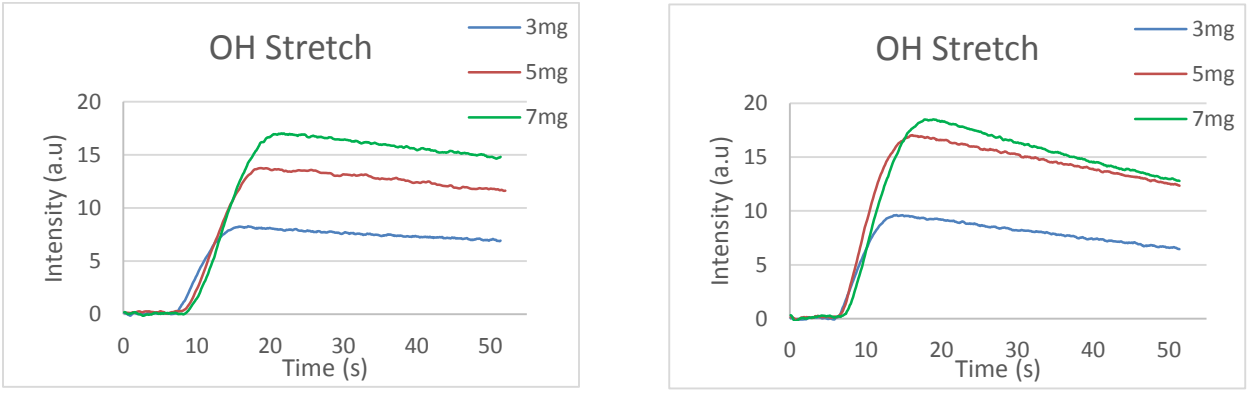

Figure C.2.1: Cellulose O-H stretch evolution with t_{res} of 0.56 s (left) and 0.38 s (right).

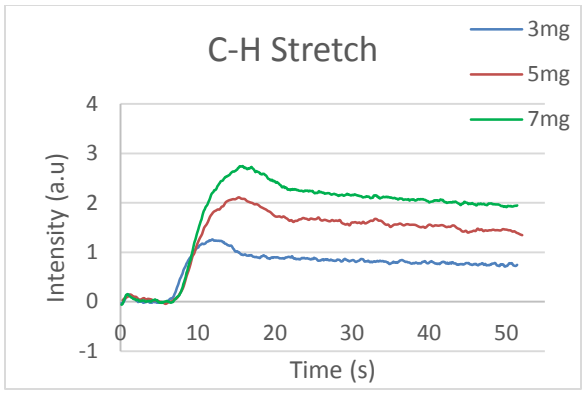

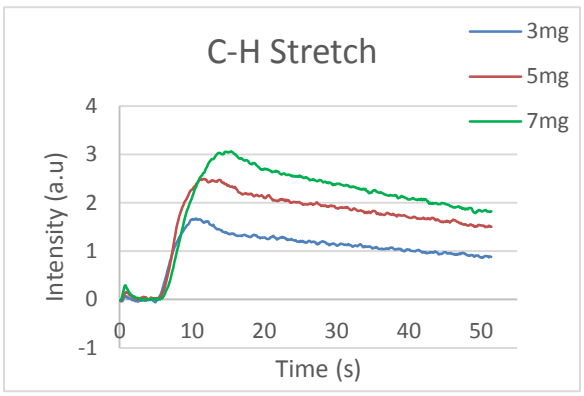

Figure C.2.2: Cellulose C-H stretch evolution with t_{res} of 0.56 s (left) and 0.38 s (right).

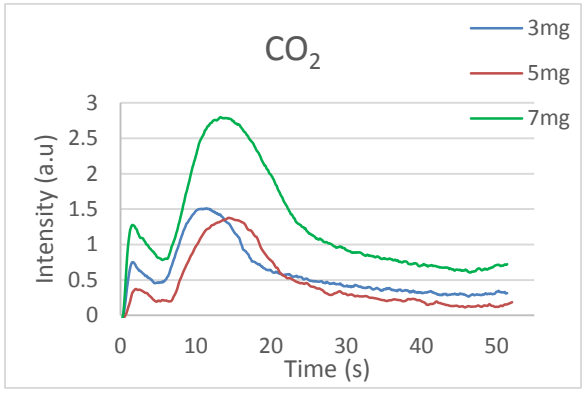

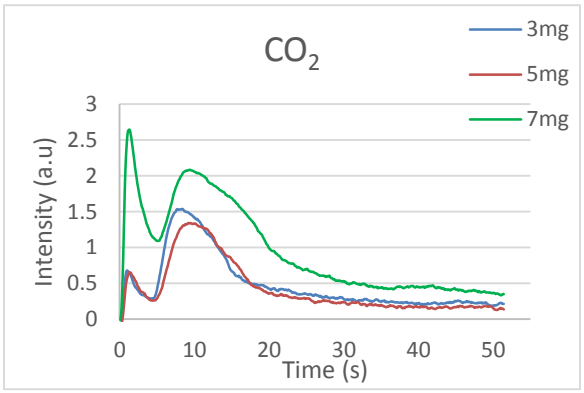

Figure C.2.3: Cellulose CO_2 evolution with t_{res} of 0.56 s (left) and 0.38 s (right).

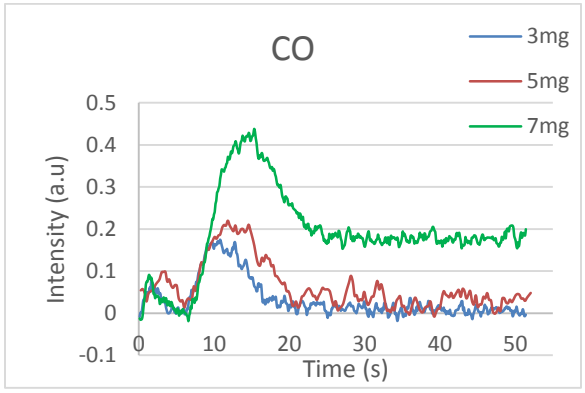

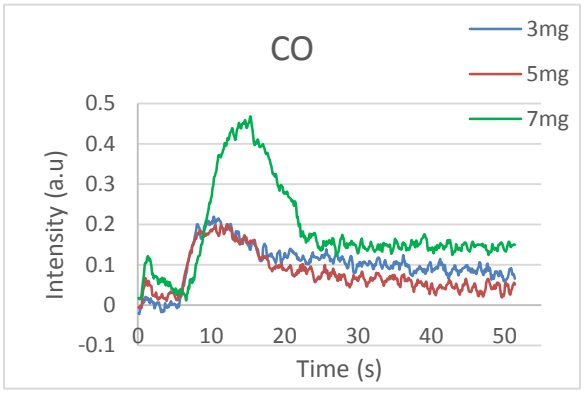

Figure C.2.4: Cellulose CO evolution with t_{res} of 0.56 s (left) and 0.38 s (right).

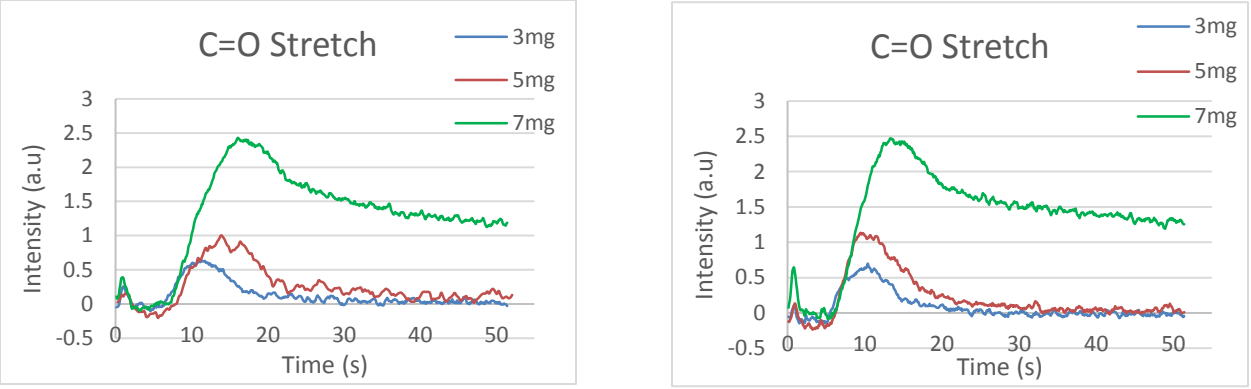

Figure C.2.5: Cellulose C=O stretch evolution with t_{res} of 0.56 s (left) and 0.38 s (right).